The effect of varying stiffness in CH-47 rotor blades on Rotor Track and Balance

M.C.H. van der Aa

Faculty of Aerospace Engineering · Delft University of Technology

The effect of varying stiffness in CH-47 rotor blades on Rotor Track and Balance

Master of Science Thesis

For obtaining the degree of Master of Science in Aerospace Engineering
at Delft University of Technology

M.C.H. van der Aa

25^{th} October 2021

Faculty of Aerospace Engineering · Delft University of Technology

The work in this thesis was supported by Netherlands Aerospace Centre. Their cooperation is gratefully acknowledged.

Delft University of Technology
Faculty of Aerospace Engineering
Department of Aerospace Structures and Materials

GRADUATION COMMITTEE

Dated: 25th October 2021

Chair holder: Dr. R.M. Groves

Committee members: Dr. A. Anisimov

Dr. ing. S.G.P. Castro

Ir. R. Brink

Abstract

The Royal Netherlands Air Force is currently operating the CH-47 helicopters as their main large transport helicopter. To improve the maintainability of rotor blades it is necessary to determine measurable parameters that can be used for matching rotor blades with similar structural properties. During the rotor track and balance (RTB) process the rotor system is balanced to reduce vibrations within acceptable limits to decrease fatigue on mechanical parts. The objective of this research is to investigate how the variation in structural properties of the rotor blades composite structure affects the dynamical response during the RTB. It is hypothesized that the variation in stiffness and shift in centre of gravity of the composite structure is caused by in-service defects and repairs. The variations caused by these non-uniformities influences the dynamical response of the rotor blade.

To achieve the research objective, a 2D analytical model based on the Classical Laminate Theory is created to quantify the change structural blade properties due to non-uniformities. This model is created to improve the rotor blade FEM models used for RTB simulations. In order to create the analytical model, detailed information about in-service defects and repairs is collected by non-destructive inspection of serviceable CH-47 rotor blades. The non-destructive inspections showed delaminations and several types of repairs were present in the rotor blades. Thermography showed to be superior over shearography for the determination of size and location of the non-uniformities, while shearography is more suitable for the detection of delaminations and but-joint debonds. The 2D analytical model calculated that a patch repair and double skin repair lead to an increase of the bending and torsional stiffness. The center of gravity shifted by limited amount due to the added weight of the applied repairs. During RTB simulations a single non-uniformity did not lead to an exceedance of the maximum vibration level. It is recommended to investigate to what extend a combination of multiple non-uniformities affect the structural blade properties.

This thesis work gives a detailed overview of what type of non-uniformities can be expected in CH-47 rotor blades. The developed analytical model can calculate the impact of a non-uniformity on the structural parameters to adjust the FEM model in RTB simulations, which contributed to further development of the Automated Rotor Blade Inspector.

Contents

List of Figures

Acronyms

ARBI Automated Rotor Blade Inspector

CFRP Carbon Fiber Reinforced composite

CG Centre of gravity

CLT Classical laminate theory

FCF Functional Check Flight

HUMS Health and Usage Monitoring System

NDI Non-destructive inspection

NLR Netherlands Aerospace Centre

OEM Origignal Equipment Manufacturer

PM Program Management office

RNLAF Royal Netherlands Air Force

RTB Rotor Track and Balance

Acknowledgments

Foremost, I want to thank Dr. Andrei Anisimov for his guidance in this process and critical questions, which helped me to further develop my own critical mindset. Special thanks to my supervisor from the NLR, Rob Brink, for the countless times he has given me feedback and advice. Even in this peculiar time he was always available to answer my questions and point me in the right direction. My sincere thanks to Dr. Roger Groves and Dr. Arjan de Jong for their feedback during key-moments in this process.

Besides my supervisors, I wish to thank the engineers from NLR: Patrick Jansen and Jacco Platenkamp for sharing their extensive knowledge in the field of NDI and support with the in-service inspections. Thanks to my colleagues within the RNLAF: Lieutenant S. Djibet, Sergeant-major R. Pieter and the engineers from the 980th Base Maintenance Squadron for discussing the rotor blade repair methods. I also want to thank my friends and colleagues Lars, Artur and Ingmar for the support, feedback and discussions along the way of my entire academic career. Without the contribution of these people I could not have accomplished this result.

Finally, I am very grateful to the RNLAF and the NLR who offered me the opportunity to participate in this project. It was an honor to help solving a problem that potentially improves the readiness of the RNLAF.

Breda, 25^{th} October 2021

Mike van der Aa

Chapter 1

Introduction

This chapter gives an introduction to the research project. Section 1.1 will introduce the main project of which this research is part of. In section 1.2 is elaborated how this research will contribute to the overall project. Section 1.3 describes the research objective. This objective will be achieved by answering the research question and sub questions that are presented in section 1.4.

1.1 Project overview

The Royal Netherlands Air Force (RNLAF) is currently operating the Boeing CH-47D and CH-47F Chinook helicopters as their main large transport helicopter. In 2021 the fleet undergoes a modernisation and upgrade program to the CH-47F MYII CAAS configuration [1]. The CH-47 Program Management office (PM) intends to keep the current rotor blades in-service on the new CH-47F MYII CAAS fleet.

To improve the maintainability of the rotor blades from the CH-47D fleet PM wants to get a better understanding of their current state and determine parameters that can be used for the formation of matching blade sets. Analysis of base maintenance data showed that the functional check flight (FCF) at the end of base maintenance inspections has the most impact on the key performance indicator: On Time Delivery. Part of the FCF is the rotor track and balance (RTB) process. During this process the rotor system is balanced to reduce vibrations within acceptable limits to increase comfort for the flight crew and decrease fatigue on mechanical parts [2]. It takes years of hands-on experience for technicians to become proficient in rotor track and balancing. Even with years of experience the technicians are sometimes unable to achieve acceptable vibrations levels with a certain combination of rotor blades [3]. It is expected that this is caused by a change in the structural properties of the rotor blades due to usage, aging and maintenance.

Every 400 flight hours the rotor blades must be thoroughly inspected and repaired when necessary. Currently, the reports of previous repairs is insufficiently detailed in the maintenance records of the RNLAF CH-47 helicopter rotor blades. There is limited historical data on the dimensions and location of the found defects and applied repairs. As a result, rotor blades end up in sets with matching in-flight behaviour to reduce the number of rotor track and balance flights. Matching rotor blade sets are formed based on an empirical process carried out by the technicians. The formation of matching sets limits the maintainability of rotor blades as they need to be kept together during inspection by the back shops. To increase the maintainability and reduce the number of rotor track and balance flights it is necessary to expand the number of measurable parameters on which the matching process is based. Therefore, it will be investigated how defects affect the structural properties of helicopter rotor blades and if these properties are relevant for the matching process.

The RNLAF contracted the Netherlands Aerospace Centre (NLR) to investigate this problem. A possible solution proposed by the NLR is the development of an Automated Rotor Blade Inspector (ARBI). ARBI utilizes non-destructive inspection (NDI) methods to determine geometrical and structural properties to match rotor blades with similar parameters. This system can be used to pre-inspect rotor blades before sending them to the composite backshop. When matching sets of rotor blades can be separated, it can speed up the inspection process and during the rotor track and balance process a new set can be formed based on measurable parameters. In the current phase of this project the NLR is carrying out a feasibility study on the development of the ARBI system.

1.2 Research context

This thesis will be part of the NLR research and development project and focus on how non-uniformities affect the structural properties of rotor blades. Non-uniformities are defined as all deviations from the designed rotor blade structure. It is expected that defects and repairs do have an affect on the weight- and stiffness-distribution of rotor blades [4, 5]. The goal of this research is to investigate how varying structural properties in the composite structure, caused by non-uniformities, affects the dynamical response of the rotor blades during the RTB process. This will be achieved by the introduction of non-uniformities on rotor blades in RTB simulations.

Section 1.1 and 1.2 gave an overview of the complete research project. The research objective of this thesis work is described in the next section. The last section contains the main research question that needs to be answered during this research to obtain the research objective. To be able to answer the main question, four sub questions are defined to support the main question.

1.3 Research Objective

The objective of this research is to investigate how the variation in structural properties of the composite structure in helicopter rotor blades affects the blades dynamical response during the RTB process. This will be achieved by improving the Finite Element Model (FEM) used for RTB simulations with an assisting 2D analytical model to determine local structural blade properties.

It is hypothesized that the variation in stiffness and shift in centre of gravity (CG) of the composite structure is caused by in-service defects and repairs. The stiffness variations caused by these non-uniformities influences the dynamical response of the rotor blade, which can explain the inconsistency between the ground vibration test results of a real rotor blade and the results obtained by a FEM model of an as new rotor blade. To limit the scope of this research the change of aerodynamic properties due to the imperfections is not taken into account during simulation.

To achieve the research objective this hypotheses will be tested by creating a 2D analytical model based on the CLT (Classical Laminate Theory) to quantify local structural blade properties and comparing RTB simulations of as new rotor blade sets to a set that contains a rotor blade with defects and/or repairs. This comparative study is carried out using a tandem rotor system model in FLIGHTLAB that is developed within the NLR's ARBI project. In order to create the analytical model, detailed information about in-service defects and repairs needs to be collected. This data will be obtained by non-destructive inspection of serviceable CH-47 rotor blades using thermography and shearography.

1.4 Research Question

The main goal of this research is to get a better understanding of how non-uniformities in the CH-47 Chinook helicopter rotor blades composite structure influence the vibration levels during rotor track and balance. Therefore the following research question needs to be answered:

- **How does the variable stiffness and change in CG of the rotor blade composite structure, caused by non-uniformities, affect the dynamical response during the rotor track and balance process?**

To answer the main question four sub questions are formed:

1. What types of in-service damage regularly occur in helicopter rotor blades and what methods are commonly used to repair those defects?

2. Which NDI methods are most suitable for characterization of important parameters as size, thickness and depth of common in-service damage and repairs?

3. How do in-service defects and repairs alter the structural blade section parameters and chord-wise moment?

4. What is the effect of defects and repairs on the vibration levels during RTB simulations?

1.5 Research outline

Chapter 2 provides the theoretical background for this thesis research. In this chapter the theory of rotor track and balance is discussed. Further is reviewed how non-uniformities in the composite blade structure affect the structural properties according to recent literature. Chapter 3 gives an overview of the theory behind the NDI methods that are used for the experiments in this research and their ability to characterize the important parameters of non-uniformities. In chapter 4 is shown how damage is modeled in the analytical CLT model and gives an overview of the theoretical framework where the model is build on. The experiments that are carried out during this research are described in chapter 5. This consist of the in-service inspection of CH-47 rotor blades, damage modelling with the CLT model and RTB simulations. The answer to the research question and the conclusions and recommendations are presented to the reader in chapter 6.

Chapter 2

Project background

This chapter gives an overview of the relevant theory that is built on during this research project. The first section focuses on the theory of rotor track and balance process. The second section looks into the effect of imperfections on composite structures and how they affect the structural properties in general.

2.1 Theory of rotor track and balance of helicopter rotor blades

Vibrations are one of the biggest problems for rotary wing aircraft. Long time exposure to excessive vibrations lead to a higher probability of failure of systems and has a negative influence on the flight crew's condition [2, 6]. The main source of these vibrations is found in the rotor system. Track and balance procedures are performed after each maintenance activity on the helicopters rotor system to minimize the level of vibrations. The track and balance process consists of 2 different techniques: static rotor blade balancing and dynamic disk balancing.

2.1.1 Rotor blade static balance

After each major inspection or repair a rotor blade must be statically balanced to compensate the change in weight distribution due to the performed maintenance actions. This is achieved by adding balance weights in the rotor blade on the feathering axis. The center of gravity can be shifted to the correct position within the limits that are described in the technical manual using a static balance fixture. In this setup a Master blade is used to calibrate the static fixture, see figure 2.1.

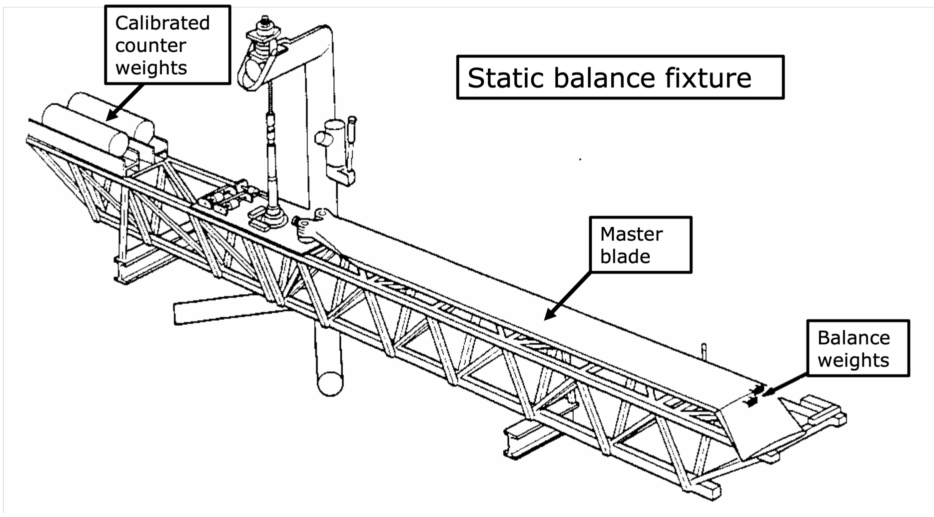

Figure 2.1: Schematic drawing of a static balance fixture [7]

This process is called spanwise balancing. The location of CG changes over time due to in-service wear and repairs. A large amount of all US Army AH-64 main rotor blade's spanwise moments were out of limits due to wear over time. The spanwise moment that is specified by the OEM (Original Equipment Manufacturer) is 24,300 inch per pound (equivalent to 2745.5 Nm). The red line in figure 2.2 shows the maximum adjustment (7 Nm or 0.2 inch per second) that can be made to the spanwise moment during dynamic balancing. Rotor blades cannot be dynamically balanced when opposing blades spanwise moment differs more than 7 Nm. A maximum scatter of up to 56,6 Nm found during spanwise moment measurements of 1100 US Army AH-64 rotor blades. Results of these measurements are presented in figure 2.2:

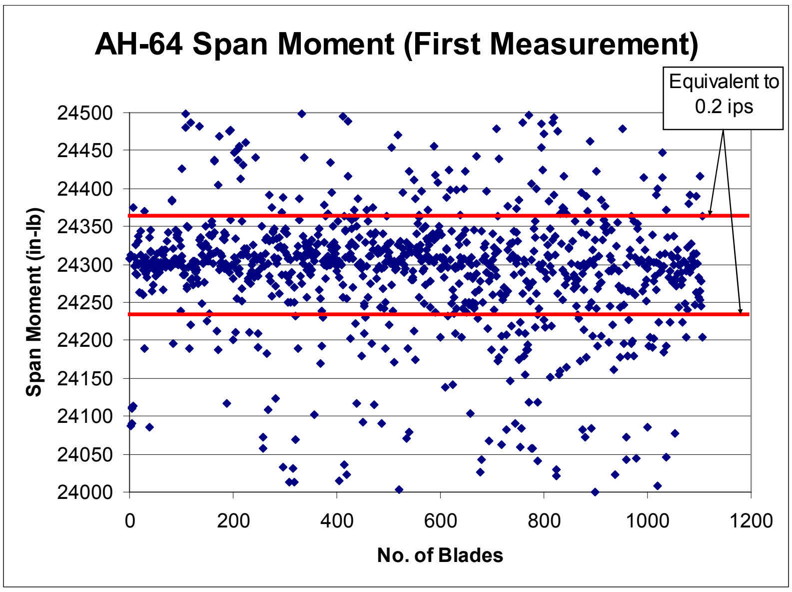

Figure 2.2: spanwise moment of 1100 AH-64 Main rotor blades[7]

This research [7] affirms that not all rotor blades can be dynamically balanced without proper static balancing. Static imbalance of a rotor blade is considered to be the origin of the majority of vibrations in the rotor system[7].

The problem of static imbalance does not only occur in helicopter rotor blades. In wind turbines it is necessary to minimize vibration excitation that could damage the wind turbine tower. The main cause of unbalance in wind turbine blades are deviations in the weight distribution of the blade [8]. These deviations can be caused by: production faults (varied material thickness), operational faults (water inside the blade or ice forming on the blade surface) or maintenance (extensive repairs). The vibrations mainly occur when the rotational frequency of the rotor disc matches the natural frequency of the tower. To minimize vibration levels weights are added to the blade root. This process is partly similar to the RTB process in helicopters.

During the literature review it seemed that static rotor balance had less scientific interest compared to dynamic balancing in the field of helicopter rotor blades. Most of RTB research is focused on developing better algorithms that select the right adjustments to decrease vibrations. Due to faster algorithms for dynamic balancing and the lack of quick static balancing methods RTB research focused more on dynamic balancing. The dynamic balancing process is explained in the next section.

2.1.2 Dynamic balancing

Dynamic balancing is divided into two sub-processes: blade tip tracking and rotor disk balancing. The flight crew and mechanics measure the tip path height of the individual rotor blades during the first part of the ground run to check if all rotor blades tips travel in the same horizontal plane. The tip height is measured with two laser range finders that are built onto the tip of the nose and the top of the fuselage [9]. The blade tip height is defined in figure 2.3:

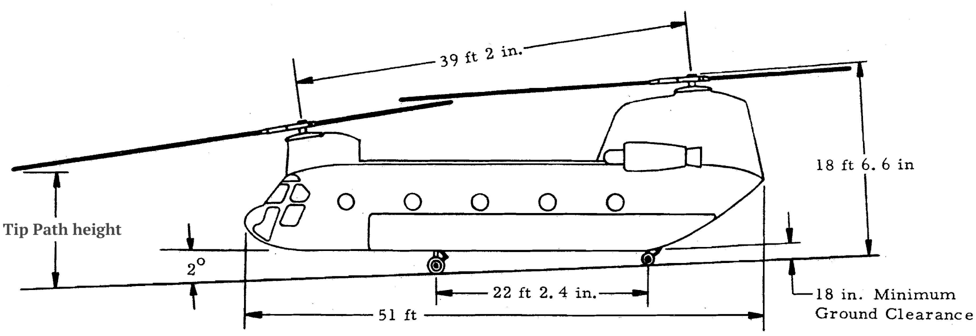

Figure 2.3: CH-47 tip path height [10]

When the blade tip height is not equal for each individual rotor blade the amount of generated lift per blade can be altered. This is accomplished by changing either the pitch rod settings or the angle of the trailing edge tabs. Changing the length of the pitch rod influences the angle of attack (α) of the blade. Bending of the trailing edge tabs is used to change the rotor blades camber profile [6]. These adjustment tools are displayed in figure 2.4:

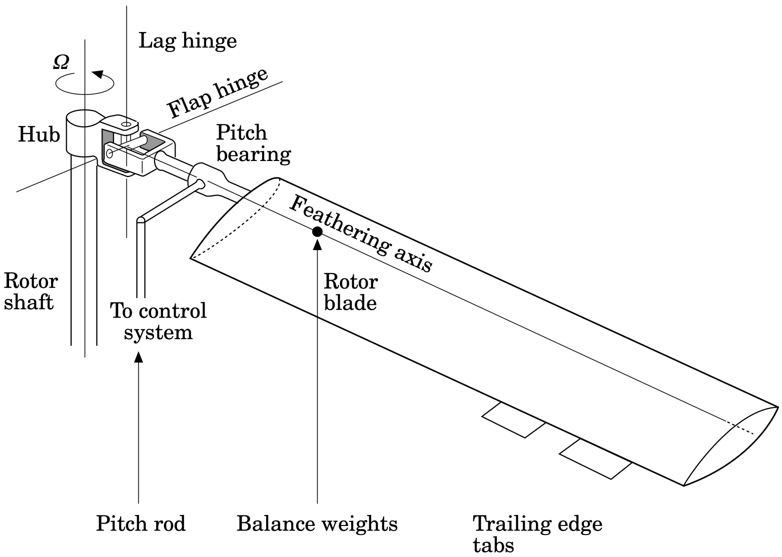

Figure 2.4: Rotor track and balance adjustment tools [6]

Maintenance procedures describe that flat track maintenance must be performed after installing new blades. However, ground crew and technicians claim that only a flat blade tip track not always results in low vibration levels [11]. The final step of RTB is rotor disk balancing. This step focuses on placing the centre of gravity of the rotor system over the center of the rotor hub in different flight regimes. In theory this should already be the case when all blades are properly statically balanced, but during the different flight speeds other aerodynamic forces disturb the rotor disk balance. The level of vibration is measured by accelerometers during three flight regimes: hover, cruising speed and high speed. The aircraft's Health and Usage Monitoring System (HUMS) contains four accelerometers for this purpose that are placed in the centre of the fuselage and on the two rotor heads. Additional adjustments of the correction parameters are proposed by an algorithm of the HUMS to reduce the level of vibrations [12].

The algorithm in the HUMS system has been developed over the past 25 years, with a main focus on dynamic balancing. The CH-47 HUMS computer collects vibration and blade track data to recommend adjustments [9]. The optimal amount and type of adjustment (or adjustment coefficients) are determined with a linear model that is derived from the basic equations of motion of a helicopter rotor system. For derivation of this model elastic deformations of the rotor blade are neglected and only quasi static aerodynamic behavior is considered. The goal of rotor track and balancing is to cancel out the effect of non-uniformities on the vibration levels by changing the correction parameters. The pitch rod settings are used to adjust the angle of attack, bending the trailing edge tabs changes cross-sectional camber and balance weights are used to change the mass distribution. An over-determined system of linear equations is obtained that is solved with the least square method. This model is used to determine the correction parameters that are most relevant in the rotor track and balance process [11]. Figure 2.5 gives an overview of the basis motions of helicopter rotor blades.

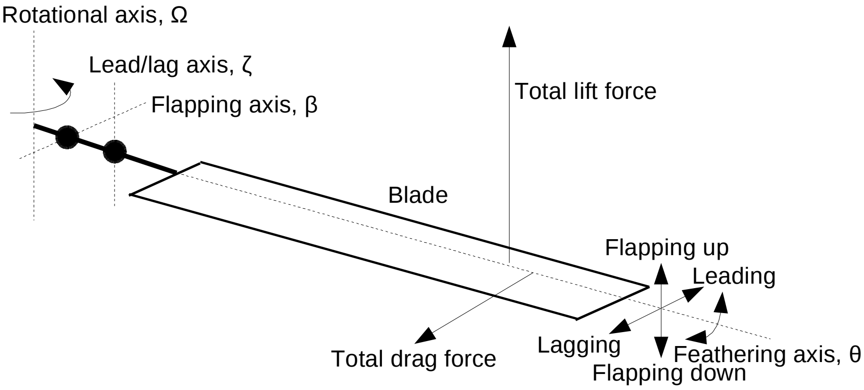

Figure 2.5: Basic motions of helicopter rotor blades [13]

The vibrations that occur in helicopters can be divided in 3 categories: "(a) high frequency vibrations, where the frequency of vibration (f) is very high compared to the rotor rotational frequency (fR), ($f > 20\ fR$)—these vibrations are mainly caused by the engine or gear-box; (b) moderate frequency vibrations ($20\ fR > f > 5\ fR$)—the tail rotor, and to a lesser extent the (main) rotor, are the main sources of these vibrations; (c) low frequency vibrations ($5\ fR > f$) that are caused mainly by the rotor. The low frequency vibrations have the most severe effect on human tolerance and fatigue of mechanical parts."[14]. The dynamic response of the blade depends on the natural frequency, damping and mode shapes. These properties are affected by defects, repairs and RTB adjustments. Blade defects can cause shift in weight distribution, airfoil shape and blade twist. The RTB procedure starts with static balancing to make sure the blades have the same location of center of gravity and inertia. During the dynamic part of RTB the pitch and airfoil can be changed by adjusting the pitch rod length and trim tabs to obtain the same track height and pitch moment. Why these properties are affected by non-uniformities is described in the next section.

2.2 The effect of non-uniformities

The properties of individual rotor blades have a significant influence on vibration levels [9]. It is hypothesized that these individual rotor blade properties are altered by non-uniformities in the composite structure of the blade. Non-uniformities are defined as all deviations from the designed rotor blade structure. This includes, but is not limited to, production faults, in-service damage and repairs. To limit the scope of this research the change of aerodynamic properties due to the imperfections is not taken into account.

Part of the goal of this research is to establish parameters on which rotor blades can be matched in sets. As pointed out in the previous paragraph the spanwise moment is important, because prior research showed that when the spanwise moment a set of AH-64 blades has a scatter over more than 7 Nm it is impossible to balance this set during dynamic RTB. The spanwise moment is determined by the mass distribution along the pitch axis of the blade. Ferrer et al. and Hillmann et al. pointed out that the dynamical properties of rotor and wind turbine blades are affected by certain defects and repairs [4, 8]. The natural frequency, damping and mode shapes have an impact the dynamical behaviour. A helicopter rotor blade can be idealised as a cantilever beam. The natural frequency (ω) of a cantilever beam is given by equation 2.1:

$$\omega = C^2 \sqrt{\frac{EI}{mL^4}} \tag{2.1}$$

Where:
E = Young's modulus
I = Area moment of inertia
m = mass per unit length
L = length of the beam
C = dimensionless constant dependant of boundary conditions

This equation indicates that the Young's modulus and mass distribution are important influence the dynamical properties of rotor blades. The stiffness of a structure depends on the Young's modulus of the material and the area and length of the structure. The moment of inertia does not change due to non-uniformities, but the stiffness and weight distribution can be affected. How non-uniformities can affect these properties will be shown in the following sub-sections.

2.2.1 Common defects in composite sandwich structures

The most common types of damage and failure modes in composites can be divided in two different categories:

- Production damage
- In-service damage

Production damage consists of defects that are caused by contamination, impact or misplacement of material in the production process. In-service damage can be caused by a wide variety of factors such as, maintenance handling, foreign object damage (bird strikes, runway debris, ballistic damage), severe operating conditions and environmental factors. A CH-47 rotor blade consists of a titanium leading edge, the center section and trailing are made of a composite structure with a honeycomb core and glass fiber reinforced polymer (GFRP) skin as is shown in figure 2.6. A schematic overview of a rotor blade structure is shown in figure 2.11.

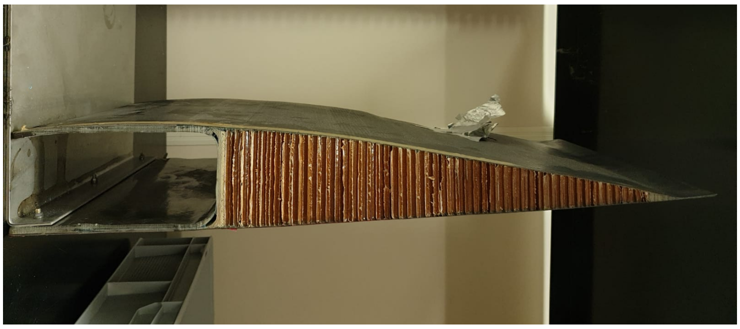

Figure 2.6: Example of a rotor blade structure with honeycomb core

Poor bonding during manufacturing between the matrix and the fibers can lead to delamination, porosities or voids in the material in composite laminates. Voids are air bubbles in the material that are large enough to be detected. A group of small voids is called porosity and when a void is filled with foreign materials it is referred to as an inclusion. In-service damage like impacts can lead to delamination or fiber-breakage. Delamination is the separation of two or more layers and is also referred to as an inter-laminar crack. This is the most common in-service defect and arises in resin enriched areas. It does not affect the tensile strength of the material, but it is more critical to compression. Fiber breakage is a trans-fibrous crack and limits the capability to transfer load along the fiber which results in a lower tensile strength of the material. These kinds of defects reduce the strength of the material and can lead to failure of the object [15]. A schematic overview of common defects is shown in figure 2.7:

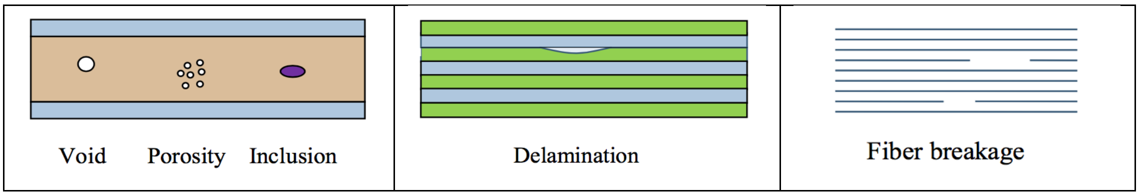

Figure 2.7: Common defects in laminated composites [15]

The most common production defects in sandwich structures are skin-core debonds and poor adhesion of butt joints. Cracks and voids can occur in foam core materials. In-service damage of honeycomb structures mainly consists of core debonds, foreign object damage and environmental factors. Impact damage can lead to internal damage of the honeycomb core structure. The most common defects in sandwich structures are shown in figure 2.8:

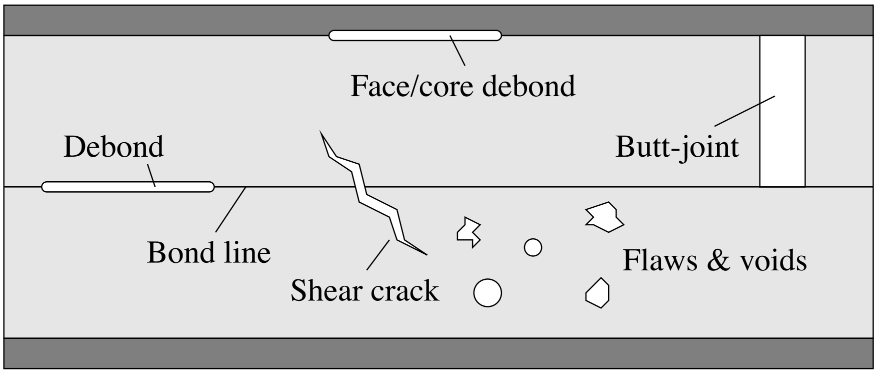

Figure 2.8: Common defects in composite sandwich structures [16]

Repairs of these common defects affect the stiffness of the composite structure. When a repair is performed part of the original structure is removed and replaced. During the repair process production defects can occur, which lower the ultimate strength. In certain cases it is necessary to strengthen the repair by adding doublers for additional stiffness.

The influence of delamination on the structural integrity of composite structures

Delamination in the composite sandwich structure leads to more friction between layers and increases the damping. The delamination also leads to a reduction in stiffness which affectd the natural frequencie of the structure. A delamination can lead to a stiffness loss of 23% for in a 4 ply lay-up and up to 48% of stiffness loss for 16 ply lay-up when a matrix ply crack evolves into a complete delamination between plies [5].

The effect of repairs on composite sandwich structures

The maintenance manual prescribes a wet lay-up patch for the repair of a delamination. This repair is of poorer quality than the base material, because entrapped air between the layers reduces the fiber volume ratio [17]. Defects to the core are mostly repaired with replacement of the core and the addition of the doubler patch as can be seen in figure 2.9. The doubler gives extra stiffness and weight to the structure, because this extra patch is added compared to the base material. Mahdi et al. [18] examined the performance of repaired composite sandwich beams. They found that the bending stiffness of repaired beams was higher in general, except for repairs with a scarf ratio over 1/30 [18].

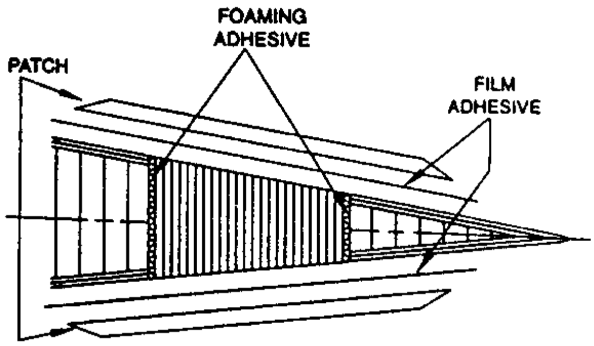

Figure 2.9: Repair of a tapered composite sandwich structure[19]

The structural repair manual of the CH-47 describes 3 types of repairs: patch repair, partial core repair and double skin repair. The patch repair is applied when the skin is damaged of a skin core debond is detected. This repair method prescribes that the original damaged or debonded skin is replaced and an extra patch is applied to secure the replaced skin. The partial core repair is prescribed when impact damage up to 1/4 of the core thickness is detected. The mechanics from the composite backshop at LCW indicated that most of the times a double skin repair is applied when impact damage is detected, because this is easier to apply. Conform the SRM, the double skin repair should be applied when the impact damage is deeper than 1/4 of the core thickness or when the damage penetrates through whole thickness of the blade. An overview of the repair methods from the SRM is given in figure 2.10.

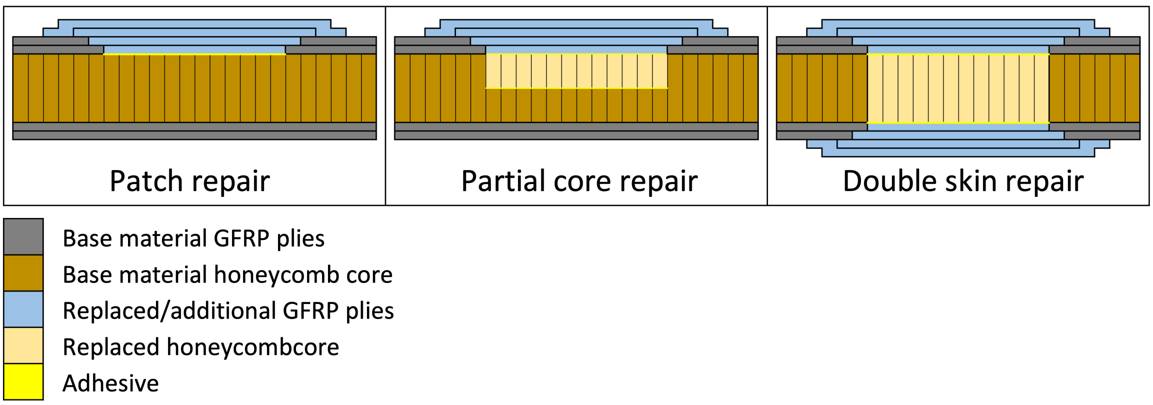

Figure 2.10: Schematic overview of repair types prescribed by the Structural Repair Manual

Butt-joint debond in helicopter rotor blades

A dangerous type of delamination can occur when water enters the honeycomb structure. When water intrudes between the honeycomb structure and spar this can lead to a debond between the core and the leading edge. The C band in figure 2.11 indicates the location of the debond:

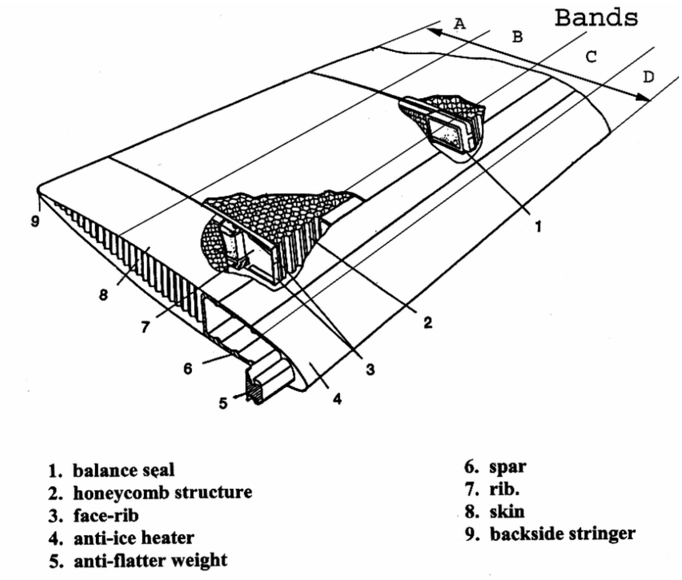

Figure 2.11: Cross-section of a general helicopter rotor blade [20]

When water intrudes this area and freezes during operation, a debond can occur due to the expansion of the water. When water is detected during inspection in this area it is less harmful, because the water can drain through the vent gap. The core-spar separation can be detected with X-ray as the image will show a double contour of the honeycomb as shown in figure 2.12. This indicates a tilted position of the core, so the core must be debonded from the spar in order to be able to tilt. When this happens the honeycomb core in this area loses its load bearing capabilities.

2.3 Conclusion

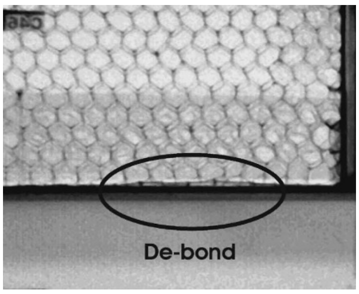

Figure 2.12: Debond of the honeycomb core and leading edge spar [21]

This chapter gave an introduction to the theory of rotor track and balance and an overview of commonly found defects and how these affect the rotor blades composite structure. This partially answers sub question 1 and 3. Delaminations reduce the stiffness of a composite laminate structure and increase the local damping. Common in service defects in sandwich structures are repaired by the addition of doubles which will increase the fiber volume ration. The butt-joint debond between the spar and core is only found in composite rotor blade structures. This defect is caused by water intrusion and can lead to a loss of load bearing capabilities across the cord length of the blade. Chapter 5 discusses the results of the non-destructive inspections. The findings of these inspections will be compared with the conclusions presented in this chapter.

Chapter 3

In-service NDI of CH-47 rotor blades

To answer the first two sub-questions, non destructive inspections are performed on serviceable CH-47 rotor blades in an operational environment at the airbase Woensdrecht. This chapter gives an overview of used NDI methods, why they are selected for this purpose and what results are of importance as input for modeling the structural blade parameters.

3.1 NDI equipment

The experimental set-up that is used for the inspection of the CH-47 rotor blades consists of a sample, a shearography and a lock-in thermography system. The PM CH-47 from the RNLAF provides the samples in the form of three in-service CH-47 helicopter rotor blades which are due for their 400 flight hour depot level maintenance inspection. The NDI equipment is provided by the NLR. Inspection of the rotor blades takes place in an operational hangar environment. Ultrasonic testing and X-ray radiography were also considered during the literature review, because ultrasonic testing is able to provide the most detailed information for the characterization of subsurface defects [22] and X-ray radiography was most suitable for the detection of butt-joint debonds [21]. However, the field of view and the inability to detect repairs limits ultrasonic testing from being used during this thesis work. The RNLAF restricted the use of X-ray radiography in a open hangar environment. In previous research [23] the NLR investigated the applicability of a system that combines shearography and thermography with a single excitation source. This is called a multi-domain NDI method. This systems combines the superior detection rate of shearography and uses thermography for characterization of the imperfections. Kalter investigated the optimal settings for damage characterization using thermography [24]. Both methods have a large field of view and can use the same excitation source to simultaneously inspect rotor blade sections. The inspection set-up is developed by Kappert during previous work within the NLR ARBI project [25]. He developed a multi-domain inspection system optimized for curved composite sandwich structures. This set-up is extensively tested in a laboratory set-up. During this thesis work the multi-domain inspection system will be used in an operational environment for the first time.

3.1.1 NDI methods for detection and characterization of imperfections in composite structures

This subsection will give an overview of the theory of suitable NDI methods for the detection and characterization of imperfections in composite structures. Inspection consists of different levels; detection, characterization and classification. First an imperfection must be detected. Characterization is the ability to measure parameters of the imperfection. Classification is defined as the ability to determine what type of defect is detected. The physics of the NDI methods will be briefly described to determine the ability of defect detection and characterization.

Thermography uses infrared radiation to detect subsurface defects. Thermal radiation of the sample is recorded with an infrared camera to obtain an image of the heat distribution over the surface of the sample. Lock-in thermography uses a heat source to excite the test sample. The heat source uses a sinusoidal input signal to radiate heat over a longer time period. The input signal is phase shifted when it penetrates the sample. When the wave encounters an imperfection the phase shifted signal is partially reflected. The reflected wave interferes with the incoming energy waves which creates an interference pattern in the surface temperature. The internal defects can be examined by evaluation of the phase shift in relation to the input signal. The ability to detect and characterize defects depends on the thermal properties of the sample and energy level of the input signal. The main advantage of thermography is the relatively large field of view ranging from 200 mm^2 to 1000 mm^2. Other advantages are that this method is contact free and does not use hazardous radiation. The disadvantage of thermography is the limited detection depth. Montanini et al. concluded that defects in GFRP laminates were detectable to a maximum depth 6 mm [27], however, the skin in CH-47 helicopter rotor blades does not exceed 3 mm thickness. Thermography does not need a coupling agent and the camera can be placed at different distances of the specimen. Repaired structures must be inspected with a non-contact and couplant-free method. Therefore, thermography is advised for inspection of repaired parts [22]. The spatial resolution of thermography is determined by the resolution of the camera that captures the image.

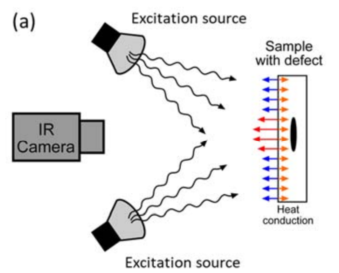

Figure 3.1: Working principle of Thermography [26]

Shearography is a non-destructive testing method that utilizes coherent laser light to examine sub-surface defects. The coherent light scatters from the rough surface and creates a stochastic speckle pattern on the surface of the sample. The speckle pattern is captured by an image-shearing camera in an unloaded state, this is called the reference frame. By applying a small load the surface

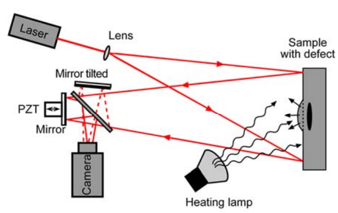

Figure 3.2: Working principle of Shearography [26]

will deform due to sub surface defects. The
light scatters in a different pattern due to surface deformations, which causes a phase difference in the intensity of the signal. The camera captures the signal frame in the loaded state. The difference between the two patterns is used to create a fringe pattern by correlation of the reference speckle pattern and the signal speckle pattern. The fringe pattern shows the derivative of the displacement of the surface in the direction of the image shearing. Advantages of shearography are the large field of view (up to 1 m^2), its relative insensitivity to noise and external vibrations, but it only provides information on the location of the defect. A drawback of shearography is that this method lacks the ability to easily determine the depth and size of the defect, but because of the large field of view and faster inspection speed, it is superior over other NDI methods [28]. Figure 3.3 gives an overview of the strengths and weaknesses of shearography and thermography.

Detection and characterization of defects	NDI method	
	Thermography	Shearography
Detection of Delamination	✓	✓
Detection of repairs	✓	✓
Detection of water ingress	✓	✕
Detection of but-joint debond	❍	❍
Defect depth	✓	✕
Thickness	❍	✕
Lateral size	✓	✓
Field of view/ inspection speed	✓	✓

Figure 3.3: Performance score of Shearography and Thermography

During previous research in the ARBI project it was shown that it is possible to characterize in-service defects under certain boundary conditions [24]. The defect depth relative to the surface and the thickness of the defect were obtained by evaluating the phase difference in the frequency domain. The peak phase frequency, peak phase difference, blind frequency and phase transition frequency of a 'normal' area are compared to an area that contained a defect. This research showed that is was possible to determine the depth of an air filled delamination based on the peak phase difference and the blind frequency, but it was only possible to obtain these results under specific conditions. Kalter states that it is very important to know the exact material properties of the base material [24]. The use of a low peak frequency with a longer duration of the heat signal makes it possible to detect defects deeper under the surface without overheating the test sample [24]. The exact material properties of the original rotor blades are not known. The material properties that are needed for the model are the materials Young's moduli, shear modulus, poison ratio and maximum strengths in tension, compression and shear. These parameters are obtained through the material data sheets of the materials stated in the SRM, but over the years the prescribed materials in the SRM changed which leaves a unknown difference between the actual material properties and the ones used for the model. This was assessed during the sensitivity analysis and a fault factor of 15% was determined for the model due to the found deviations. The results of the sensitivity analysis are discussed in detail in section 4.2.3. During the in-service inspection a few environmental effects impacted the inspections. The compressor of the nearby located painting dock caused vibrations that interfered with photogrammetry and shearography images. For photogramatry the pictures were out of focus and in the shearography there was already a distortion in the specle pattern before excitation with the heat source. A few pictures had to be taken again when this was discovered and the compressor was shut down. Wind gust in the hangar environment impacted the results of thermography inspections. The ambient temperature was not constant which was visible on the thermography images, by altering the frames for background filtering, images of equal quality were obtained. However, it was not possible to apply the method suggested by Kalter for depth estimation of defects. By combining the thermography images with the repair options from the SRM it was possible to determine the type of repair that was applied. The next sections give a detailed description of the equipment that is used for the in-service NDI.

3.2 Thermography

The lock-in thermography system is produced by Edevis OTvis and consists of a FLIR SC7600 infrared camera and two halogen light sources to heat the test sample, see figure 3.5a. The halogen lamps provide 4 kW output power. The infrared camera has a maximum resolution of 640x512 pixels and a sampling rate of 100 Hz. The camera uses a lens with a fixed focal length of 25 mm to capture infrared light in the mid wave infrared band with wavelengths between 3.4 - 4.9 μm. The FLIR SC7600 camera uses a sensor with a pixel spacing of 15 μm [29]. The data is processed with Edevis DisplayIMG software. Images were shot at different frequencies. Frequency selection was done by testing different frequencies on a calibration panel that contained artificial defects [23]. For frequencies below 0,1Hz there was no phase difference detected between the defect and the original material. At 0,1Hz the signal to noise ratio increased and showed a clear image of the artificial defect. The images captured at this frequency show more details of the honeycomb core material. At higher frequencies the signal to noise ratio decreased, but the image revealed more details of the skin. The penetration depth of the heat signal depends on the thermal properties of the material and of the frequency of the modulation wave. The penetration depth is defined as the thermal diffusion length μ:

$$\mu = \sqrt{\frac{k}{\pi f \rho c_p}} \tag{3.1}$$

Where:
k = Thermal conductivity
c_p = specific heat
ρ = density
f = selected frequency

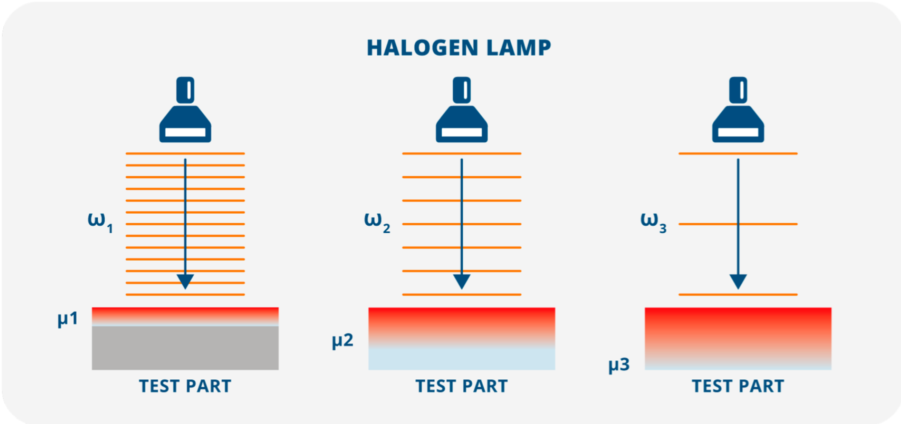

Figure 3.4: Schematic diffusion length for different frequencies. Courtesy of NLR

Figure 3.4 shows the effect of the frequency on the penetration depth. A lower frequency excitation signal results in a higher penetration depth and provides more information on defects deeper in the sample. Therefore, inspection of the skin area was performed at 0,8 Hz with a heat excitation of 8 seconds at 95% of the maximum power output. In the following 20 seconds, the heat flux of the sample was imaged to measure the phase difference. To look deeper into the material a frequency of 0,1Hz was used. The sample was radiated for 1 second at 75% of the maximum power output with an acquisition time of 8 seconds.

3.3 Shearography

For shearography a 5 mega pixel Isi-sys SE2 sensor is used. The sensor is equipped with a Sigma EX lens. The sensor has a maximum frame rate of 15 Hz and the focal length of the lens is 35 mm. The same halogen lamps are used for the sample excitation. The system uses two isi-sys diode laser array as coherent light source. Each array includes five diodes with an 100 mW output per diode. This system is showed in figure 3.5b:

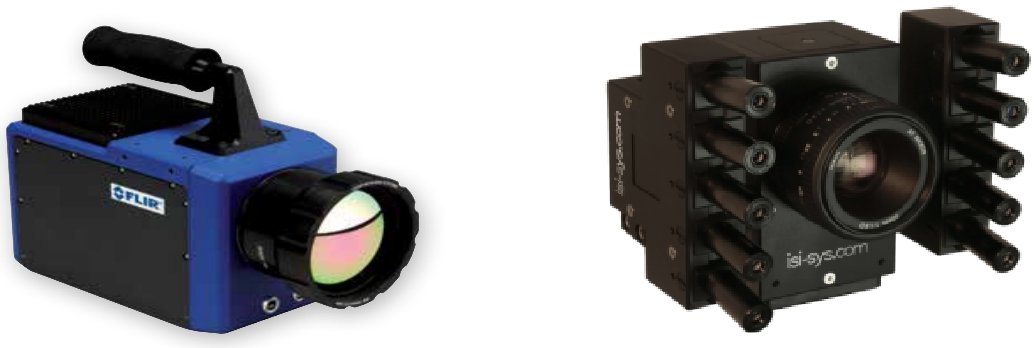

(a) FLIR SC7600 infrared camera [29]

(b) Isi-sys SE2 shearography system [30]

Figure 3.5: NDI systems

For the shearography the sample is also radiated with a 1 second pulse at 75% of the maximum power output of the halogen lamps. The reference image is captured directly after the pulse.

The displacement is captured for 25 seconds after the pulse at 5 frames per second. The 32nd frame was used for background filtering and a shear factor of 5mm was applied.

3.4 Test set-up

During the in-service inspection of CH-47 rotor blades shearography and thermography will be used complimentary to each other. The complete setup is shown in figure 3.6. For both methods the FOV is 1000x750x750 mm and is accurate to 0.05 mm [31], indicating that between 10 and 15 pictures are needed to get an image of the complete rotor blade. To be able to stitch the images together photogrammetry is used to create a 3-D image of the rotor blade. Stickers on the rotor blade are used as a reference for the stitching process of the shearography and thermography image which is done in the GOM inspect suite software. The size and location of the imperfection are determined by overlaying the NDI images on the 3D model. The dimensional data of defects and repairs gathered during NDI will be used as input data for the CLT model. The length, width and location of the repair are directly used from the NDI images. Dattoma et al. [32] state that it is not possible to characterize the nature and dimensions of defects by thermography alone. They developed a procedure for classification of common defects in composite sandwich structures by applying artificial defects. A list was created were the defects are linked to the corresponding thermal response. This list was used to obtain a handbook for the identification of defects in sandwich structures in wind turbine rotor blades. While this method cannot be used for the in-service inspection of helicopter rotor blades, because it is not certified in the maintenance manual, a similar approach is used during this research. A list of common repair methods from the SRM were linked the thermal response on the NDI results based on maintenance records and expertise of the technicians.

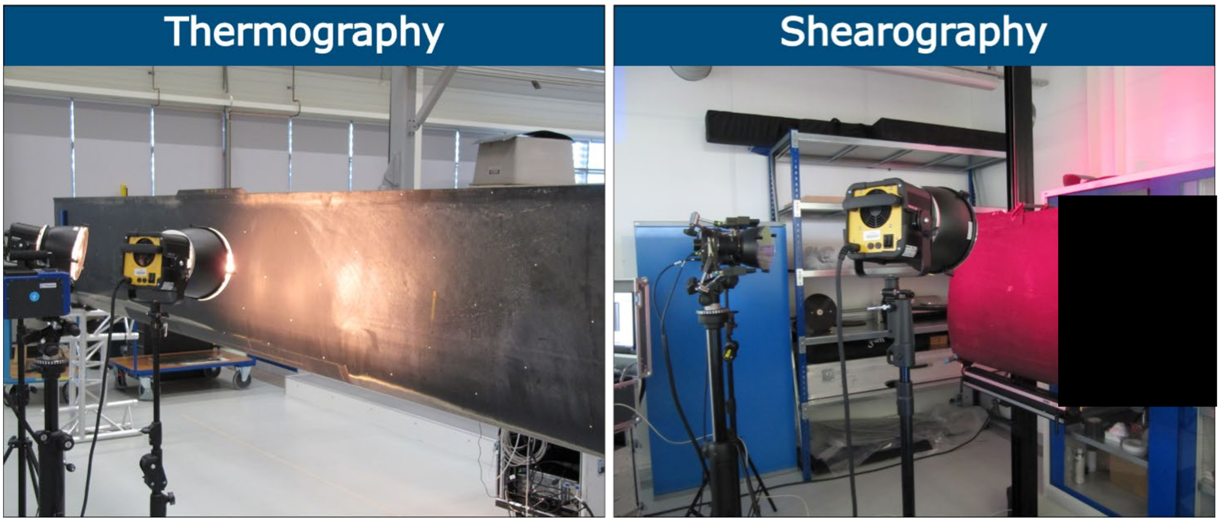

Figure 3.6: In-service non-destructive inspection of a CH-47 rotor blade at NLR

3.5 Conclusion

The findings of chapter 2 and 3 provide an answer to the first sub question. In chapter 2 it was already shown that delaminations, skin-core debonds and butt-joint debonds are the most common defects that are found in composite sandwich structures. Delaminations and skin-core debonds lead to significant reductions in local stiffness. Repairs of these defects increase the local stiffness when a doubler patch is applied in the repair method. This chapter provides an overview of the NDI methods that were used during this research. It was shown that thermography and shearography both can be used for the detection of delaminations and repairs. In theory thermography is more suitable for the determination of the lateral size and location of the non-uniformities. In chapter 5 it will be shown that it is necessary to use both NDI methods as the shearography detected certain defects that were not shown in the thermography results at the higher frequency.

Chapter 4

Modeling of non-uniformities

This chapter gives an overview of the model that is used for the modeling of non-uniformities. The model is developed to evaluate the relevant structural properties that are used to model rotor blades for RTB simulations.

At the NLR a 3D FEM model is used for the simulation of RTB [31]. Commonly 3D FEM models for rotor blades use boundary conditions based on beam theory's like the Timoshenko or Euler-Bernoulli theory [18, 33, 34, 35]. Modeling with the Timoshenko beam theory results in larger deflections and therefore lower eigenfrequencies of the structure compared to the Euleur-Bernoulli theory. This is caused by the added deformation mechanisms. The Timoshenko beam theory does not assume that the normal plain remains perpendicular to the mid-plan like the Euler-Bernoulli theory. In practice the Timoshenko beam theory gives a better estimation for the eigenfrequency of short beams. For slender beams, like rotor blades, there is no significant difference between the eigenfrequencies determined by use of the Euler-Bernoulli and Timoshenko theory [36].

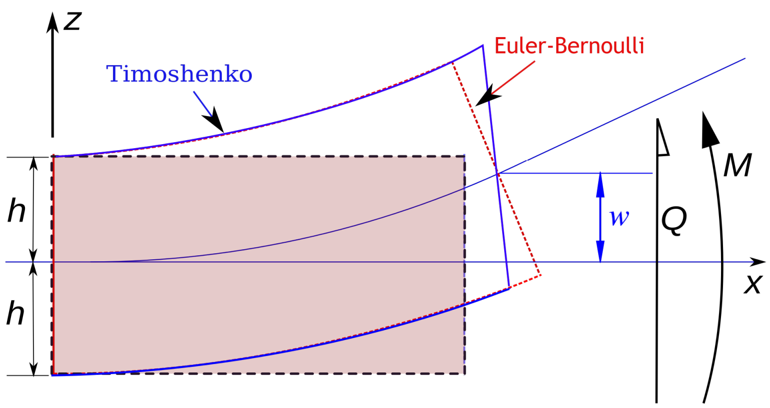

Figure 4.1: Shear deformation in the Euler-Bernoulli theory vs the Timoschenko beam Theory

Mahdi et al. [37] advise to develop a 2D plain strain model to examine the effect of non-uniformities on the stiffness of composite structures. They validated this method by comparing the flexural stiffness of repaired beams obtained by the 2D model with 3D modeling and bending tests. The results showed that the 2D model closely approximated the results obtained by 3D modeling and the bending tests [18]. The main advantage of a 2D model is that it accurately calculated these properties based on individual material properties. For modelling of repairs this approach is very suitable because, each repair can differ in material composition and geometry. When only a 3D FEM model is used, there is a need to determine the local structural properties of sections that contain imperfections by testing. With the assisting 2D model testing is not necessary as the repair geometry and material parameters are known. The 2D model can calculate the local structural parameters based on those input values. Another advantage is that the 2D model will need significantly less computational power to calculate the stiffness of the repaired structure compared to the 3D model.

During this research a 2D plain strain model is developed to evaluate the defects and repairs in more detail. The analytical 2D model is used to improve the 3D FEM model. The local in-plane and flexural stiffness are calculated with the analytical model and the results are projected on the elements of the FEM model. In the next sections the theoretical basis that is used for the development of the analytical 2D model is described.

4.1 Modeling of composite structures

The 2D model is build on the foundations of the Classical Laminate Theory (CLT). The Classical Laminate Theory is based on the on the Kirchhoff-Love theory of plates. CLT can be applied to flat structures of which the thickness is very small compared to the length and width and are made of linear elastic materials, which is the case in composite laminates and sandwich cores [38]. In the CLT plates that represent the individual lamina are modelled with the Kichoff-Love theory and stacked together to create a laminate. This method streamlines the inclusion of defects and repairs. Defects can be modeled by adding plates with an (infinitesimal) small stiffness to simulate inclusions and delamination. Doublers of repairs can be incorporated by the local addition of extra lamina to the laminate.

4.1.1 Kirchoff-Love Theory

The CLT finds its origin in the Kichoff-Love theory for plates. Love developed a two-dimensional model to calculate the stresses and deformations of thin plates when subjected to a force. This theory can be used to determine continuous displacements of the mid plane surface and global material properties. The Kirchhoff-Love theory is based on the Euler-Bernoulli beam theory. Love modified this theory with kinematic assumptions devised by Kirchoff to modify the Euler-Bernoulli beam theory for application on thin plates.

Kirchoff made three assumptions. The thickness of the plate is assumed to remain consistent during deformation. This means that there is no extension in the transverse direction ($\varepsilon_{zz} = 0$). The outer edge of the plate is assumed to remain perpendicular to the mid-plane after deformation, so transverse shear is neglected. In figure 4.2 is shown that after deflection the plane AD remains perpendicular to the neutral axis in point B ($\varepsilon_{xz} = 0$, $\varepsilon_{yz} = 0$).

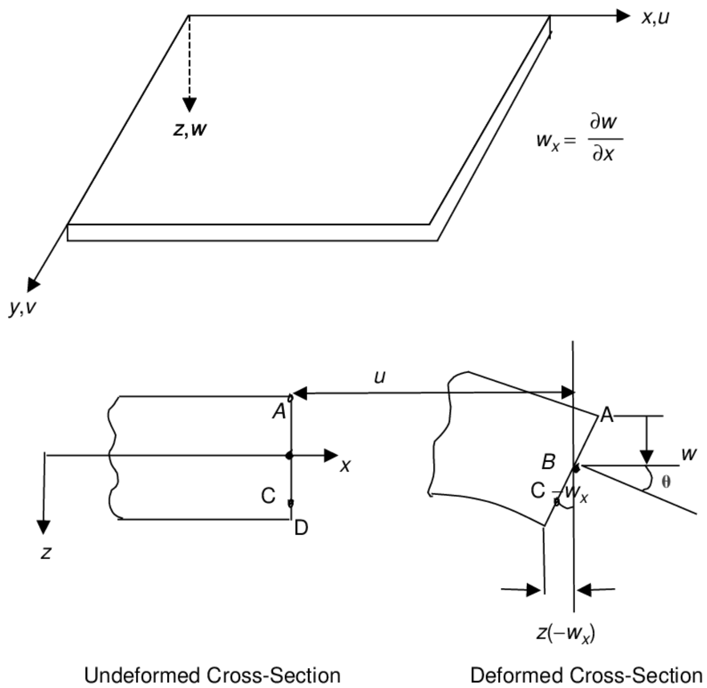

Figure 4.2: Deformations in the Classical Plate Theory

The displacement field of the Kirchhoff-Love theory is described with the following equations:

$$u = u_0 - z(\frac{\delta w}{\delta x}) \tag{4.1a}$$
$$v = v_0 - z(\frac{\delta w}{\delta y}) \tag{4.1b}$$
$$w = w(x, y) \tag{4.1c}$$

From equation 4.1a-c can be concluded that the in-plane strain has a linear relation with the thickness. The strain can be calculated with the following equation when the rotation $\theta < 10°$:

$$\varepsilon_{xx} = (\frac{\delta u}{\delta x} - z\frac{\delta^2 w}{\delta x^2}) \tag{4.2a}$$
$$\varepsilon_{yy} = (\frac{\delta v}{\delta y} - z\frac{\delta^2 w}{\delta y^2}) \tag{4.2b}$$
$$\varepsilon_{xy} = \frac{1}{2}(\frac{\delta u}{\delta y} + \frac{\delta v}{\delta x}) - z\frac{\delta^2 w}{\delta x \delta y}) \tag{4.2c}$$

With the help of Hooke's Law the general stress-strain relation for an an-isotropic linear elastic plate can be written in vector notation by:

$$\sigma_{ij} = Q_{ijkl}\varepsilon_{kl} \tag{4.3}$$

Where Q_{ijkl} is the local stiffness matrix of the plate. The next section explains how the CLT derives the global material properties of a laminate that is build out of different lamina.

4.1.2 Classical laminate theory

Composite sandwich structures usually consist of a skin and core structure. Where the skin can be built out of one or more composite lamina. In the CLT every individual lamina or core is modelled as an plate. The material properties of a laminate are determined by the properties and orientation of the individual lamina. When the material properties of individual plies is unknown, these can be calculated using the rule of mixtures (equation 4.4).

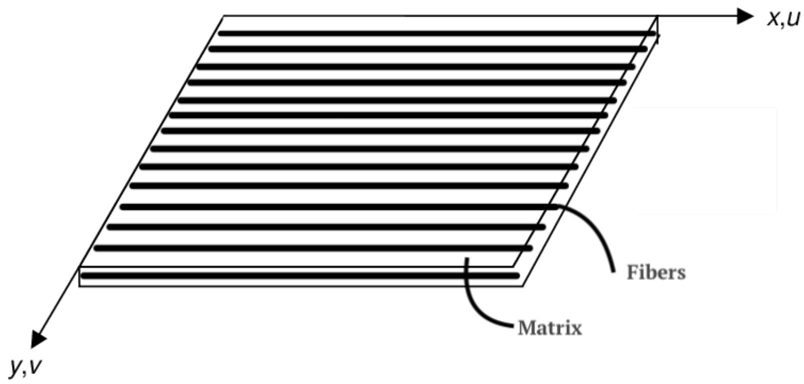

Figure 4.3: Deformations in the Classical Laminate Theory

The rule of mixtures uses the material properties of each individual material and the volume fraction to calculate the elastic properties of a fiber reinforced composite lamina. The Young's moduli (E_i), shear moduli (G_{ij}) and Poisson's ratios (v_{ij}) are calculated with the following set of equations:

$$E_1 = (1-f)E_m + fE_f \tag{4.4a}$$
$$E_2 = E_m \tag{4.4b}$$
$$G_{12} = G_m = \frac{E_m}{2(1+v_m)} \tag{4.4c}$$
$$v_{12} = (1-f)v_m + fv_f \tag{4.4d}$$
$$v_{21} = v_{12}(\frac{E_2}{E_1}) \tag{4.4e}$$

Wherein the subscripts f and m respectively indicate the material properties of the fibers and the matrix. These material properties are used to obtain the local stiffness matrix Q_k for each individual k^{th} lamina. The an-isotropic nature of composite materials requires the calculation of the material properties in the global direction of the laminate, which depends on the fiber orientation. The local stiffness matrix is given in equation 4.5. The global stiffness matrix $\overline{Q}$ is obtained by transformation of the local stiffness matrix Q_k using transformation formulas (equations 4.6a-f) to incorporate the fiber orientation.

$$[Q]_k = \begin{bmatrix} Q_{11} & Q_{12} & 0 \\ Q_{21} & Q_{22} & 0 \\ 0 & 0 & Q_{66} \end{bmatrix} = \begin{bmatrix} \frac{E_1}{1-v_{12}v_{21}} & \frac{E_1}{1-v_{12}v_{21}} & 0 \\ \frac{E_1}{1-v_{12}v_{21}} & \frac{E_2}{1-v_{12}v_{21}} & 0 \\ 0 & 0 & G_{12} \end{bmatrix} \tag{4.5}$$

$$\overline{Q}_{11} = Q_{11}cos^4\theta + 2(Q_{12} + 2Q_{66})sin^2\theta cos^2\theta + Q_{22}sin^4\theta \tag{4.6a}$$
$$\overline{Q}_{22} = Q_{11}sin^4\theta + 2(Q_{12} + 2Q_{66})sin^2\theta cos^2\theta + Q_{22}cos^4\theta \tag{4.6b}$$
$$\overline{Q}_{12} = (Q_{11} + Q_{22} - 4Q_{66})sin^2\theta cos^2\theta + Q_{12}(sin^4\theta + cos^4\theta) \tag{4.6c}$$
$$\overline{Q}_{66} = (Q_{11} + Q_{22} - 2Q_{12} - 2Q_{66})sin^2\theta cos^2\theta + Q_{66}(sin^4\theta + cos^4\theta) \tag{4.6d}$$
$$\overline{Q}_{16} = (Q_{11} - Q_{12} - 2Q_{66})cos^3\theta sin\theta - (Q_{22} - Q_{12} - 2Q_{66})cos\theta sin^3\theta \tag{4.6e}$$
$$\overline{Q}_{26} = (Q_{11} - Q_{12} - 2Q_{66})cos\theta sin^3\theta - (Q_{22} - Q_{12} - 2Q_{66})cos^3\theta sin\theta \tag{4.6f}$$

The CLT uses these global stiffness matrix to compose the ABD-matrix of the laminate. The ABD matrix consists of the Extension Stiffness Matrix (A_{ij}), the Extension-Bending Coupling Matrix (B_{ij}) and the Bending Stiffness Matrix (D_{ij}). The A, B, and D matrices are defined as:

$$[A_{ij}] = \sum_{k=1}^{n} [\overline{Q}_{ij}]_k t_k \tag{4.7a}$$
$$[B_{ij}] = \sum_{k=1}^{n} [\overline{Q}_{ij}]_k t_k \overline{z}_k \tag{4.7b}$$
$$[D_{ij}] = \sum_{k=1}^{n} [\overline{Q}_{ij}]_k (t_k \overline{z}_k^2 + \frac{t_k^3}{12}) \tag{4.7c}$$

Where:
k = lamina number
n = total number of lamina
t_k = thickness of the k^{th} lamina
$\overline{z}_k$ = distance to mid-plane

The values of these matrices determine the (coupling) effects of deformation under loading. The mid-plane strain and curvature are calculated withe the following equation:

$$\begin{Bmatrix} N \\ M \end{Bmatrix} = \begin{bmatrix} A & B \\ B & D \end{bmatrix} \begin{Bmatrix} \varepsilon \\ \kappa \end{Bmatrix} \tag{4.8}$$

Where:
N = applied force on the laminate
M = applied moment on the laminate
ε = laminate mid-plane strain
κ = laminate mid-plane curvature

4.2 Modeling of non-uniformities in helicopter rotor blades

The theory of CLT will be used to develop a MATLAB model to determine the structural properties of sandwich structures. The model must take the variable lamina thickness and different material properties of the materials in the CH-47 rotor blade into account. Damage modeling with the CLT has not been done before, therefore the last section of this chapter describes the method for the incorporation of non-uniformities and the validation of the MATLAB model.

4.2.1 Variable thickness

As shown in equation 4.7 the ABD matrix depends on the lamina thickness and distance of the mid-plane of the lamina to the mid-plane of the laminate. The thickness of the laminate h is defined as the sum of the individual lamina. $\overline{z}_k$ can than be calculated with:

$$\overline{z}_k = \sum_{k=1}^{n} t_k - \frac{h + t_k}{2} \tag{4.9}$$

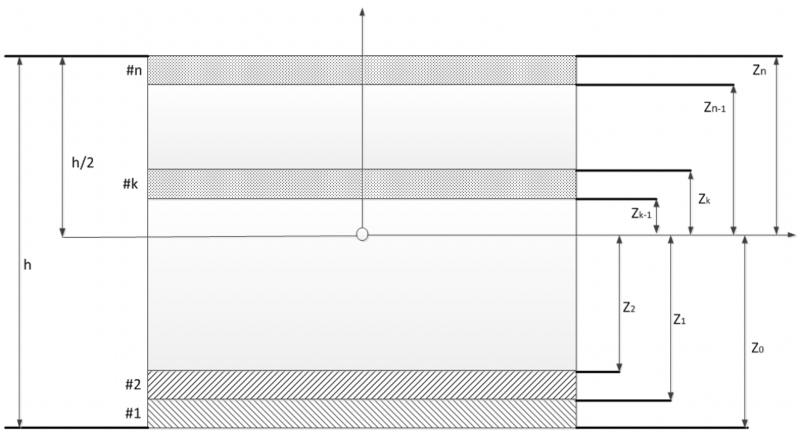

Figure 4.4: Definition of CLT variables *(reprint from lecture slides TU/Delft "Design and analysis of composite structures" by Zarouchas)*

This takes into account the variable thickness of the different materials in the rotorblades structure. The variable lamina thickness also has an effect on the engineering constants. When the ABD matrix is known, the global material properties can be calculated with the following set of equations:

In-plane engineering constants:

$$E_x = \frac{1}{h * [A_{11}]} \tag{4.10a}$$

$$E_y = \frac{1}{h * [A_{22}]} \tag{4.10b}$$

$$G_{xy} = \frac{1}{h * [A_{33}]} \tag{4.10c}$$

$$v_{xy} = -\frac{[A_{12}]}{[A_{11}]} \tag{4.10d}$$

$$v_{yx} = -\frac{[A_{12}]}{[A_{22}]} \tag{4.10e}$$

Flexural engineering constants:

$$E_x = \frac{12}{h^3 * [D_{11}]} \tag{4.11a}$$

$$E_y = \frac{12}{h^3 * [D_{22}]} \tag{4.11b}$$

$$G_{xy} = \frac{12}{h^3 * [D_{33}]} \tag{4.11c}$$

$$v_{xy} = -\frac{[D_{12}]}{[D_{11}]} \tag{4.11d}$$

$$v_{yx} = -\frac{[D_{12}]}{[D_{22}]} \tag{4.11e}$$

4.2.2 Non-uniformities

Delaminations in composite sandwich structures mostly occur as a debond between the skin and the core. For the simulation of a delamination in experiments often a teflon insert is used. The material properties of Teflon are 1/1000 times smaller than the material properties of carbon fiber. So, delaminations will be modelled as an additional lamina with an infinitesimal small stiffness to simulate a debond. A fiber breakage can also cause a delamination. Fiber breakage is hard to detect with NDI, therefore a delamination will be modelled as a debond with infinitesimal small stiffness and a load bearing lamina will be replaced with a ply with the material properties of the matrix. Patch repairs can be taken into account by modelling extra lamina on top of the skin. Core repairs are incorporated by adding an extra lamina to represent the adhesive layer and different properties of the honeycomb core if applicable.

4.2.3 Sensitivity analysis

The model is validated with 3 different test cases. For each case the composite structure's material properties are calculated with the model and the results are compared with the material properties obtained from testing to validate the model and determine the sensitivity to different input values. The three cases consist of a CFRP (Carbon Fiber Reinforced Composite) laminate, a CFRP laminate with a stepped repair and a sandwich structure.

The sensitivity of the model is tested by changing the input parameters and comparing the scatter of the output. For the first two results the input of the material parameters varied from -15% to +15% compared to the value of that parameters on the material data sheet for a CFRP laminate with a [45 -45 0 90]s lay-up. A difference of up to 5% in material properties and up to 2° deviation of the ply orientation can occur due to the uncertainty of the material data sheet data. The higher deviations are tested to incorporate manufacturing faults like a higher/lower fiber volume, use of overdue materials or offset in ply orientation during hand lay-up. A total of 8 different data inputs are simulated with an offset to test the sensitivity of the model. From left to right; the first line of triangles resembles the output by a change in input of the lamina Young's modulus in the 0 direction (E_1), the second set is the lamina's Young's modulus in the 90 direction (E_2). The third line of triangles represents the outputs for a variation in shear modulus (G_{12}). The squares represent the results of the calculations where a combination of parameters is varied from -15% to +15%. The circles represent the calculations where the ply orientation is varied from 1° to 5° offset from the initial orientation. The first 5 results represent a shift in the 0/90 orientated plies, for the other cases the orientation of the +45/-45 plies is shifted.
Figure 4.5 also shows that a variation of 30% in the input values for E_1 results in a similar percentage difference in the outcome of the calculated bending modulus. A 30% variation of E_2 and G_{12} result is a scatter of 1% and 4% on the corresponding output values of the bending modulus (flexural E_x). The same effect can be seen in the case were a combination of input values is altered. The case were E_2 and G_{12} are varied gives the same results as the case of G_{12}. So, it can be concluded that the scatter of the outcome of the bending modulus is mainly affected by the shift in E_1. In this scenario the model seems insensitive for a shift in the input of E_2, this effect is observed due to the ratio between E_f and E_m as can be seen in equation 4.4. From equation 4.7 to 4.11 can be derived that the laminates flexural E_x (bending modulus) only depends on the local stiffness when the thickness of the lamina is constant. E_f » E_m, therefore a small variation of E_m has little influence on the outcome of the bending modulus. The shift in ply orientation of the [0 90] plies by 5° results in an decrease of the bending modulus by 1%. An offset in the [+/-45] has a negligible effect on the bending modulus, this is expected from equation 4.6.

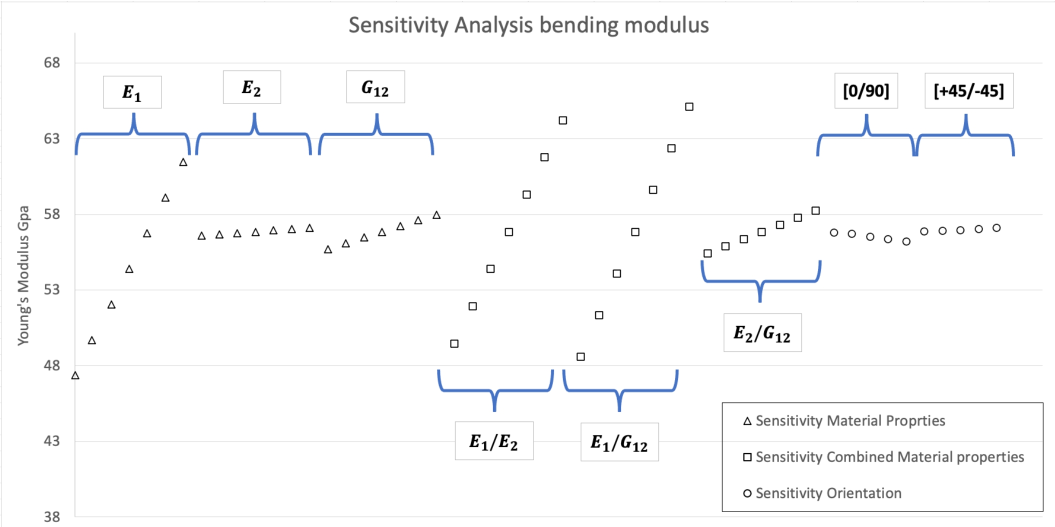

Figure 4.5: Sensitivity analysis of varying input parameters on the bending stiffness

Figure 4.6 shows similar results for the effect of the input data to the outcome of the shear modulus (in plane G_{xy}). One factor that stands out is that a shift of ply orientation of the [+/-45] plies decreases the shear modulus. This can be explained by the fact that [+/-45] plies have a better resistance to shear stress which increases the shear modulus of the lay-up. When is deviated from this ideal lay-up the resistance to shear stress decreases.

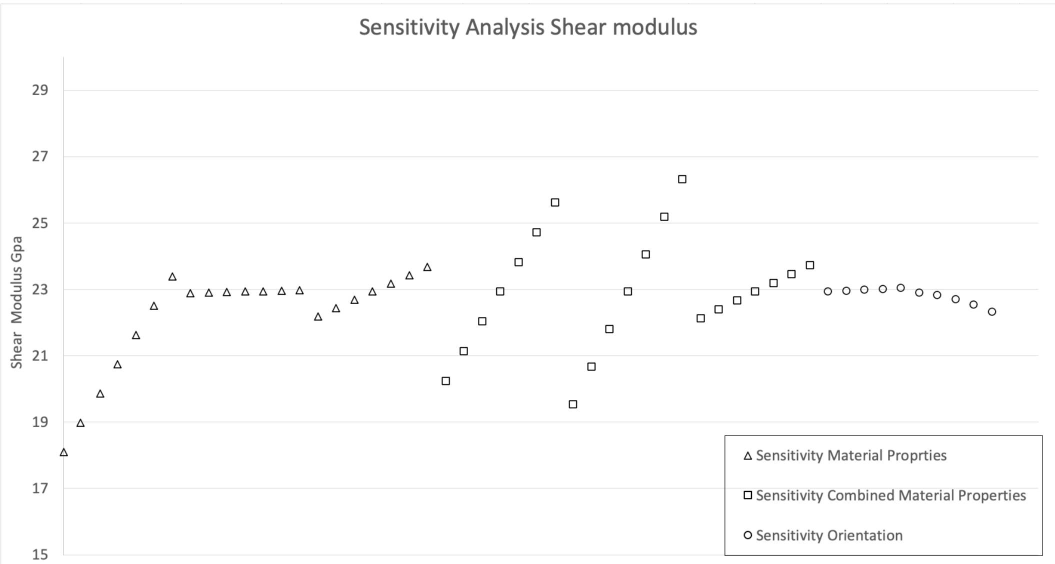

Figure 4.6: Sensitivity analysis of varying input parameters on the shear modulus

With this sensitivity analysis is shown that the scatter of the outcome is in line with a deviation of the input data when the lamina thickness remains constant. In the following figure is shown how different composite structures react to a variation of the lamina thickness. To check the sensitivity for the change in thickness the same monolithic CFRP sample was modelled as well as a sandwich structure with the same laminate as the monolithic sample, but combined with a honeycomb core. The thickness of the plies and core was varied from the initial ply thickness off 0.125 mm to determine the impact on the bending and shear modulus.

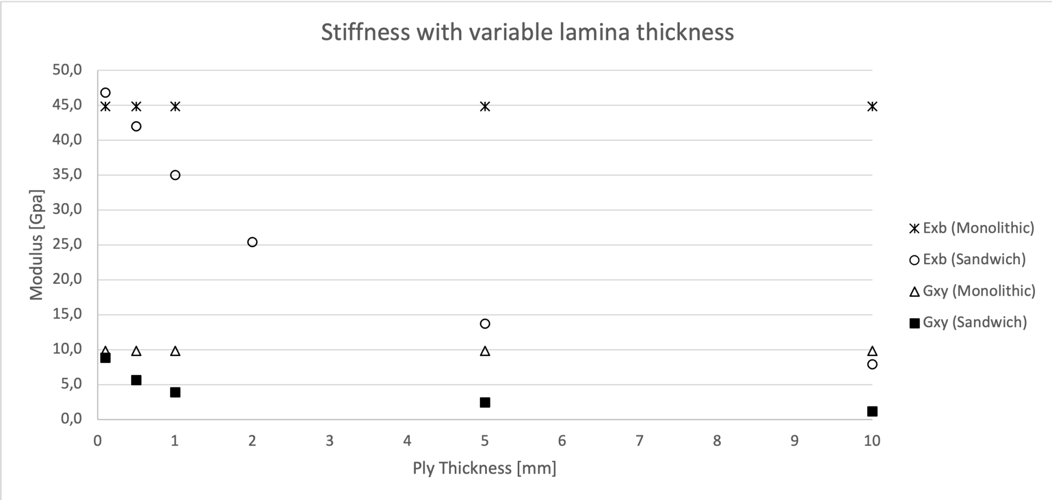

Figure 4.7: Sensitivity analysis of varying core thickness on the flexural stiffness and shear modulus

In figure 4.7 is shown that a variation in the ply thickness does not affect the output in the case of a monolithic material, which confirms the previous conclusion. When the thickness of the honeycomb core is increased the bending and shear moduli converge to the value of the modulus of the honeycomb core when the core thickness is 80 times larges than the ply thickness.

Case 1: CFRP sample

To validate the model, tension tests are performed on standard and repaired CFRP specimens. The tension tests are performed to determine the Young's modulus of the material and compare the test results to the Young's modulus predicted by the model. Figure 4.10 shows the results of the tension test. A 99,7% confidence interval determines the scatter of the data. The model predicts that the E-modulus of this material is 54,40 GPa. During the sensitivity analyses was found that a scatter in material properties can result in a maximal error of 15%. The material that is used for the production of the test sample was 2 months overdue at the time of manufacturing. The fact that the sample was manufactured by an inexperienced engineer can lead to production faults such as entrapped air and deviation of the ply orientation. The sensitivity analysis showed that the a deviation of the ply orientation $< 5°$ does not lead to a major effect on the material properties predicted by the model. The results of the tension tests performed in the CFRP sample are presented in figure 4.10

Figure 4.8: Tension test of a CFRP laminate with [0 90 45 -45]s lay-up

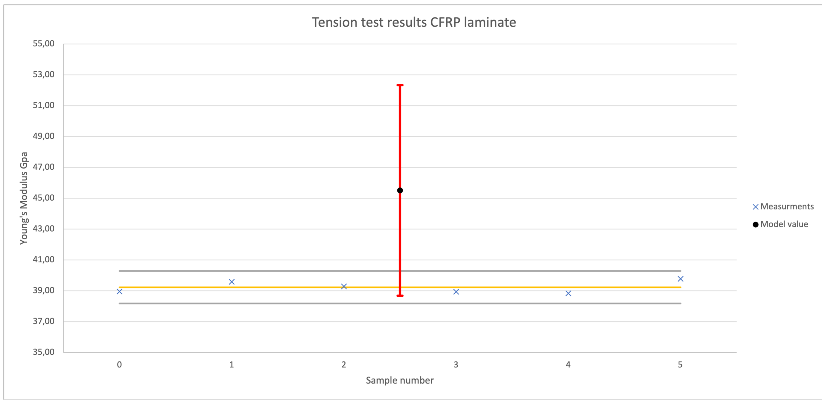

Figure 4.9: Tension test results of a CFRP laminate with [0 90 45 -45]s lay-up

The tests resulted in a mean value for the Young's modulus of 42,32 $\pm$ 2,355 GPa, that means that the the initial value calculated by the model overshoots the measured material parameter by 28,5%.

Case 2: Repaired CFRP sample

An identical CFRP laminate is produced for the tests is case 2. This laminate was impacted with a spherical impactor to create an impact damage. The damaged area was removed and replaced with a scarf repair to create a repaired CFRP sample that is similar to the laminate of case 1.

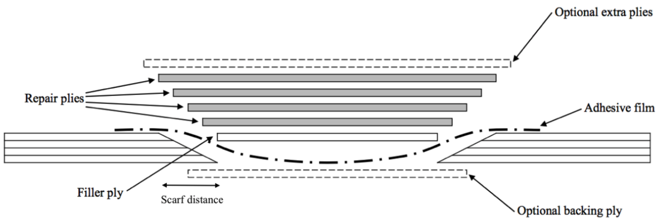

Figure 4.10: Schematic layout of a bonded scarf repair [17]

After the application of the repair the center strip of the laminate is used for testing. The test resulted in a maximum tensile stress of 382,22 Mpa, the measured strain was 0,0135. The Youngs modulus is calculated with Hooke's law:

$$E = \frac{\sigma_{max}}{\epsilon} = \frac{382{,}22}{0{,}0135} = 29,40GPa \tag{4.12}$$

The model returned a value of 37,52 GPa. This is 27,6% higher than the measured value. The overshoot of the model prediction of the measured value is probably caused by degradation of the pre-preg material that is used for the test sample and the introduction of imperfections like voids and inclusions during the manufacturing process which weakens the sample. The fact that the overshoot is constant shows that the model works accurately as the used material and manufacturing process was similar for both cases.

Case 3: Sandwich structure

The third validation case focuses on a sandwich structure. In this case the material data sheet of honeycomb core structures did not include the Young's modulus but only the shear and bending modulus, because the main advantage of using honeycomb materials is their ability to withstand shear stresses. When the Young's modulus of a honeycomb structure is unknown the value can be calculated with the rule of mixtures in a modified form. The volume of the cell material is calculated from the relative cell density and geometry and multiplied with the Young's modulus of the core materials in solid state. The second part of the equation is equal to 0 as the second medium in a sandwich structure is air. The Young's modulus of a honeycomb core can than be written as:

$$E_1 = \frac{4}{3}(\frac{t}{l})^3 E_s \tag{4.13}$$

Where t is the thickness of the core material and l the length of a cell wall. This equation is only valid for small deformations, linear elastic behaviour of the cell wall and the contribution of shear to the deformation is neglected, which is in line with the assumptions made in the Kirhcoff-love theory of plates. The test data for a 3-point bending test of a carbon-fibre/honeycomb sandwich panel was obtained from a test report [39]. The sandwich structure is simulated in the model as a honeycomb core with skin sheets in a [0 90 0] orientation.

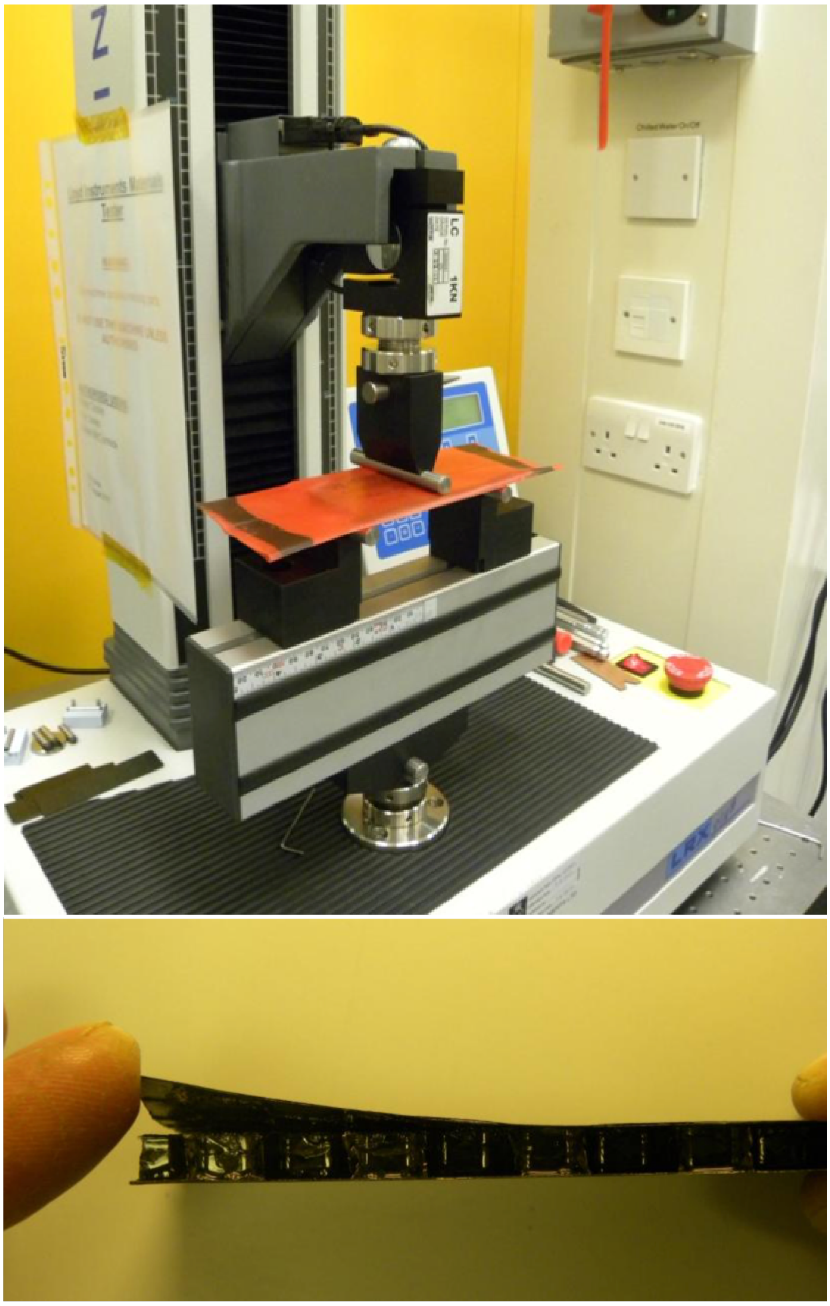

Figure 4.11: 3 point bending test of a carbon fibre sandwich structure

The mean value of the flexural stiffness of the 3-point bending test was 8,39 ± 0,957 Gpa. The model calculated a value of 9,31 GPa. As shown in the sensitivity analysis the bending stiffness of a sandwich structure could vary over 15% due to a difference between the real material properties in relation to the properties stated on the data sheet and manufacturing defects, which are neglected in the model.

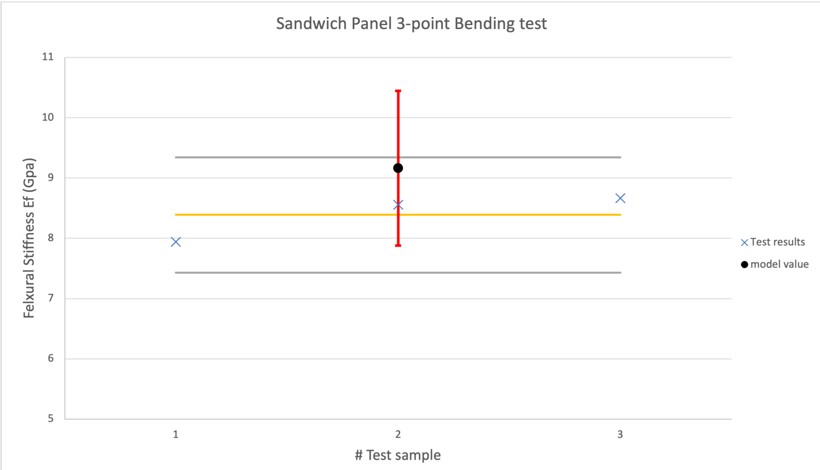

Figure 4.12: 3 point bending test results of a carbon fibre sandwich structure

4.3 Conclusion

This chapter gave an overview of the theoretical framework on which the 2D CLT model is built. The model is validated with a tension test for a monolithic CFRP sample and a carbon fibre sandwich panel. For both tests the model showed consistent results. In the case of the CFRP sample the model overshoots the measured value by 28%. This difference most likely originates from a deviation between input values of the material properties and the actual material properties of the overdue CFRP pre-preg that was used during manufacturing of the sample. Also, the fact that the sample was produced by an inexperienced engineer could have led to an offset of fiber orientation and entrapped air in the sample, which lower the maximum tensile strength. In the case of the sandwich structure the model overshoots the mean measured value by 14%, this overlaps the confidence interval of the test set data.

Chapter 5

Experiments

This chapter describes of the experiments that are carried out during this research project. To get the relevant input parameters for the model a series of non-destructive inspections of operational CH-47 rotor blades were performed. The rotor blades were inspected using thermography and shearography. The results of these inspections are used to model the rotor blade with the help of the 2D analytical MATLAB model. The output of the modified CLT model is used to improve the rotor blade FEM model. The last section gives an overview of the RTB simulations that are conducted with FLIGHTLAB to determine in-flight vibration levels of the modified FEM model.

5.1 NDI results

A complete set of 3 CH-47 rotor blades is inspected before entering the RNLAF composite repair shop for the 400 hours main rotor blade inspection and repair. During these inspections three key imperfections were found:

- Delaminations
- butt-joint debond
- Double skin Repair

Delamination

According to the maintenance manual defects are allowed up to an area of 6,45 cm^2. When a delamination grows beyond this point it needs a repair. Two delaminations were found during inspection. One of which could not be detected with the conventional inspection method (coin tapping) prescribed in the maintenance manual. Figure 5.1 gives an example of the delaminations that were found.

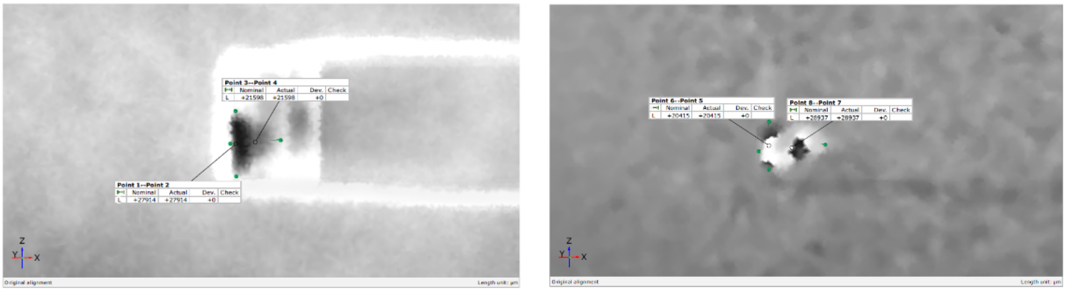

Thermography of Delamination region
Frequency: 0,8 Hz Amplitude: 95% Pulse time: 8s Aquisition time: 20s

Schearography (Horizontal) of Delamination region
Pulse time: 1s Amplitude 75%(of 4kW) Frame rate: 5Hz Shearfactor: 5mm

Figure 5.1: Thermography (left) and Shearography (right) images of a delamination region

In figure 5.1 can be seen that in the shearography image the delamination is clearly distinct from the base material. In the thermography image the delamination shows also the adhesive layer that is applied to adhere the skin patch to the base material. The size of the delamination is measured with the internal measurement system in the GOM inspect suite software. The measurement points are placed manually. While the edges of the delamination in the shearography image are less obvious the length and width measurement only differ 1 mm when compared to the thermography image.

Method	Delamination length	Delamination width
Thermography	27,9 mm	21,6 mm
Shearography	28,9 mm	20,4 mm
Visual	28 mm	21 mm

The input of the cross section blade parameters calculated by the model is limited by the amount of elements in the blade FEM model. To keep the computational time within a acceptable limits the amount of elements require that the input data is implemented with an accuracy of 10 mm. With the resolution of the camera of 5MP (2580x2048 pixels) and a FOV of 1000x750 it is possible to determine the size of a defect with an accuracy of 0,4 mm. Both images are usable for the determination of the input data, but the thermography image gives a clearer image of the shape of the delamination.

Butt-joint

Another defect that was not detected by conventional inspection methods was a butt-joint debond. The shearography image of a section of a blade showed a rim in the chord-wise direction. There was no visible indication of a defect and on the 0,8 Hz thermography images was nothing visible at that location. After the complete inspection of the blade this area was reinspected with thermography at a lower frequency of 0,1 Hz. These images also showed a lighter line in the same location. When zoomed in on the honeycomb core material a crushed core similar to figure 5.3 was observed. A scrapped rotor blade test sample was disassembled to check the internal structure. At this area 2 pieces of core were adhered together, which explains the crushed core. Horizontal shearing of this section caused the rim in the shearography image.

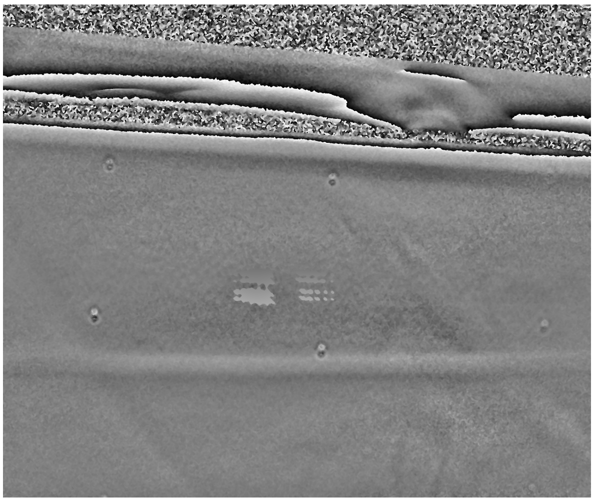

Figure 5.2: Example of a shearography image of a butt-joint debond indication (rim) [40]

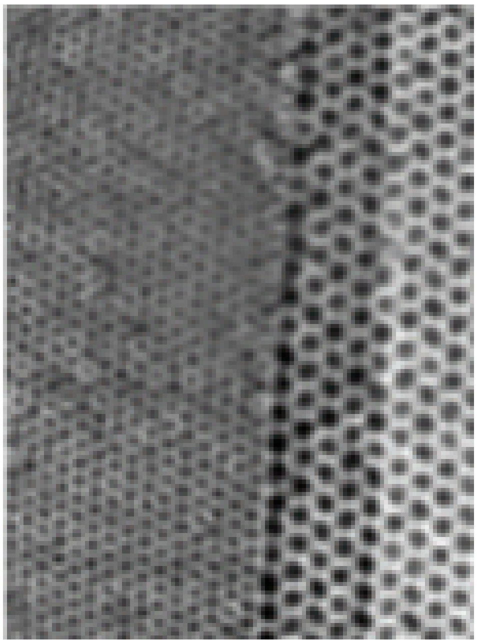

Figure 5.3: Example of a thermography image of a core density transition in honeycomb core

Repairs

Double skin repairs are visible with the naked eye as the added patch lays on top of the base material on both sides of the rotor blade. During the NDI inspections 2 double skin repairs were found. Both were measured in the analysis software based on the thermography and shearography image. The variation in the measurements were 18 and 5,7 mm respectively. This variation was caused by the manual placement of the measurement points. In the thermography image the edge of the patch is a distinct line while in the shearography image this edge was visible as a wider blurry line. The midpoint of the blurred line was assumed to be edge of the patch.

Method	Measurement patch 1	Measurement patch 2
Thermography	206,1 cm	6,32 cm
Shearography	207,9 cm	6,89 cm
Visual	206,3 cm	6,4 cm

These measurements were checked with a tape measure to determine the inaccuracy of both methods. This was only possible for the two repairs that were visible at the surface. Thermography seems most suitable for the determination of size and location of the defect. The size measured from the thermography images is within the 10 mm limit accuracy that is needed for the input data of the model. Shearography can be used as an additional method for the detection of small defects and butt-joint debonds.

5.2 Simulation of the effect of non-uniformities

5.2.1 CLT model simulation

This section gives an overview of the results that are gathered from the CLT model. The model calculates the percentual increase of the most important parameters per defect and type of repair to give a general overview of the impact of these non-uniformities. For the simulation a rotor blade composite sandwich structure was modelled. The skin is modelled in accordance with the material properties of HexForce 1581 glass with the Hexply F155 resin compound and is oriented in a [0 90 45 -45] lay-up. The honeycomb core consists of Hexcel Core HRH-10-3.2-123 which are adhered to the skin with a Hexbond Adhesive [41]. A delamination with fibre breakage, patch repair, partial core repair and a double skin repair are modeled in this structure.

Figure 5.4 gives an overview of the impact on the flexural stiffnesses and torsional stiffness as a function of the core thickness divided by the skin thickness. The actual rotor blade structure varies from minimal ratio of 2,05 to 34,4.

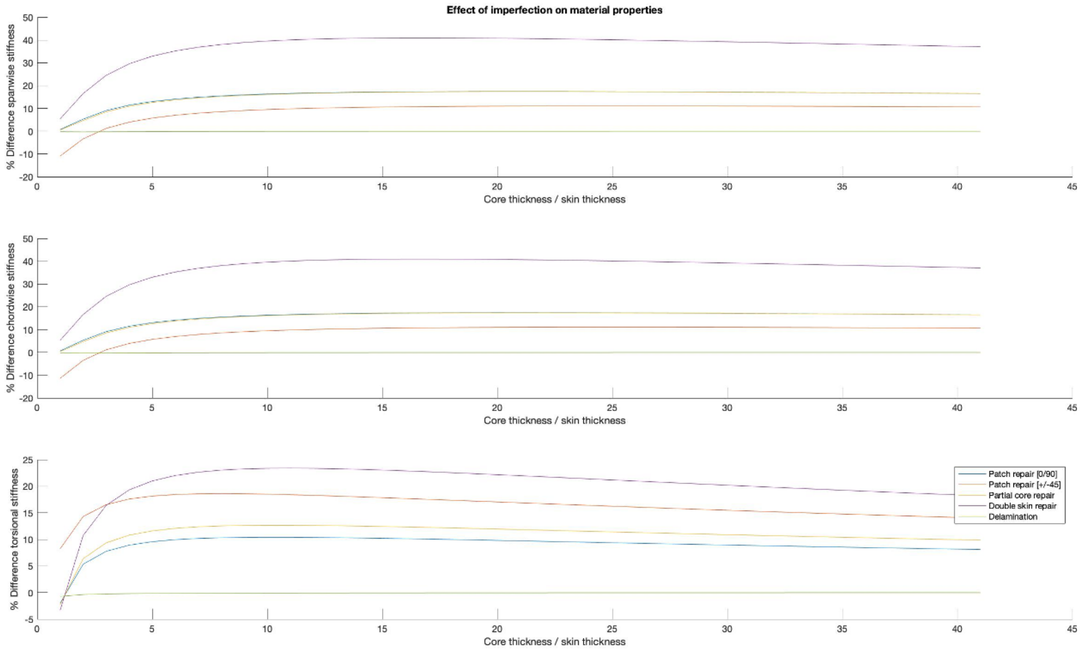

Figure 5.4: Overview of percentual impact of non-uniformities on rotor blade structural parameters

From these simulations can be concluded that the decrease in flexural and torsional stiffness due to a delamination is limited to -1%. A patch repair where the [0 90] plies are replaced with a [45 -45] patch decrease the bending stiffness when the core thickness/ skin thickness is smaller than 2,4. When the core thickness increases, the flexural stiffness is raised by 9%. By replacing the [0 90] layers the overall torsional stiffness is also increased, because [45 -45] plies are better resistant to shear. The partial core repair and [0 90] patch repair have a similar effect on these parameters, however the effect of the partial core repair is underestimated by the model. In the partial core repair a layer of adhesive is added between the two parts of the core. The induced peak stresses are not taken into account in this model. Only the Young's and Shear moduli of the adhesive are incorporated. The double skin repair has the largest impact on the stiffnesses which is caused by the addition of extra skin plies. The addition of fiber reinforced skin plies increases the overall volume fraction of the fibers, which have a significantly larger Young's and Shear modulus compared to the honeycomb core material.

The stiffness per core thickness / skin thickness ratio is used to simulate the defects and repairs that were found during the in-service NDI of the rotor blades. In consultation with the mechanics, three non-uniformities were chosen for the RTB simulation. The first one is the delamination, because this is the most common defect that is found during inspection. The second one is a [0 90] patch repair, as this is the most used repair method. The last case is a large double skin repair. This repair was considered the worst case scenario and is expected to have the largest impact on the cross sectional parameters. The defects that are analysed for further analysis are shown in figure 5.5:

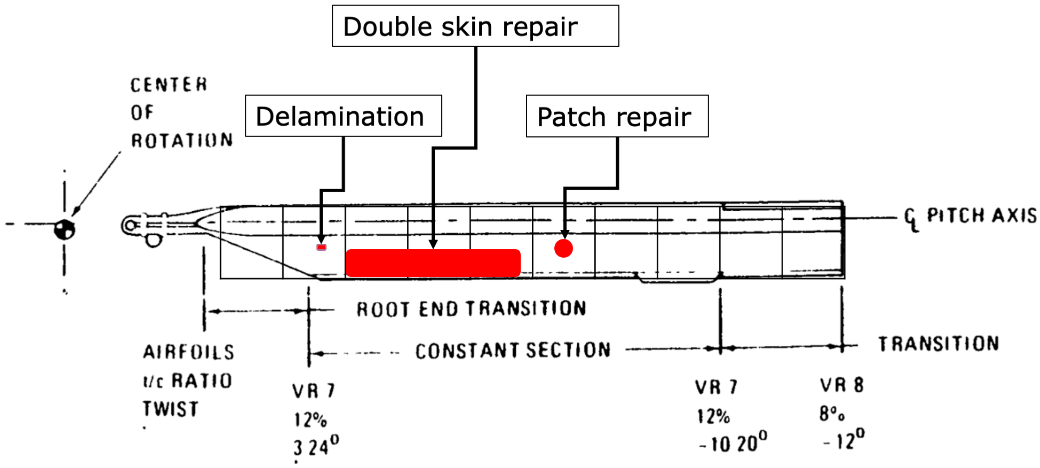

Figure 5.5: Defect map of non-uniformities found during in-service NDI [42]

Note that not all non-uniformites were encountered in the same blade, but for convenience they are displayed on the same rotor blade defect map. The following figures show the change in cross sectional parameters due to these non-uniformities. The orange dotted line resembles the cross sectional modulus when the defect or repair affects the whole chord length. The grey line indicates the actual cross sectional modulus that will be used as an input to the FEM model. The stiffness of the nodes at the location of the repair are altered in accordance with the output of the CLT model.

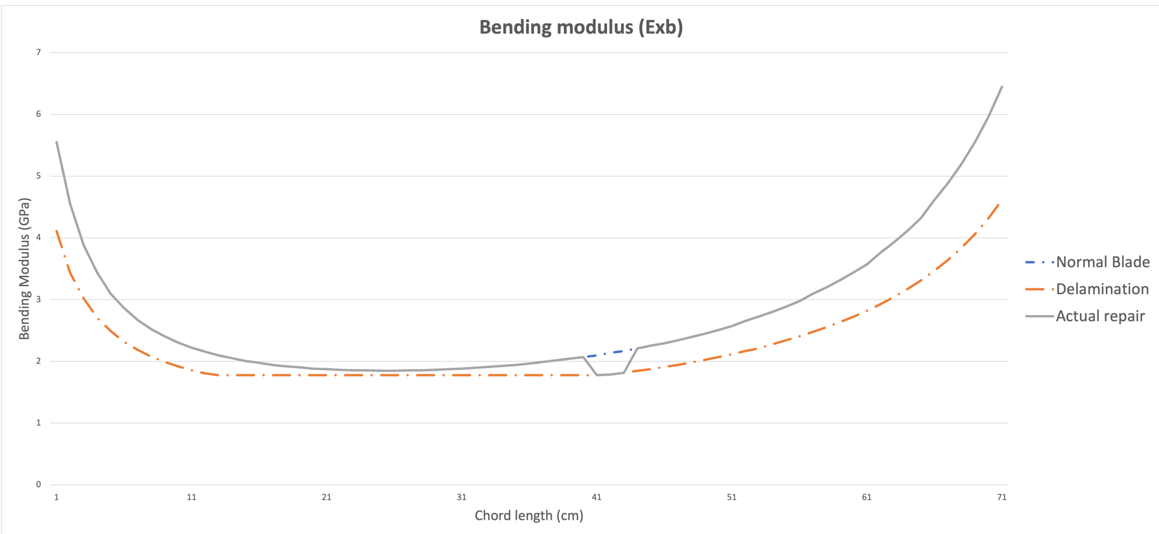

Figure 5.6: Cross sectional bending modulus with delamination

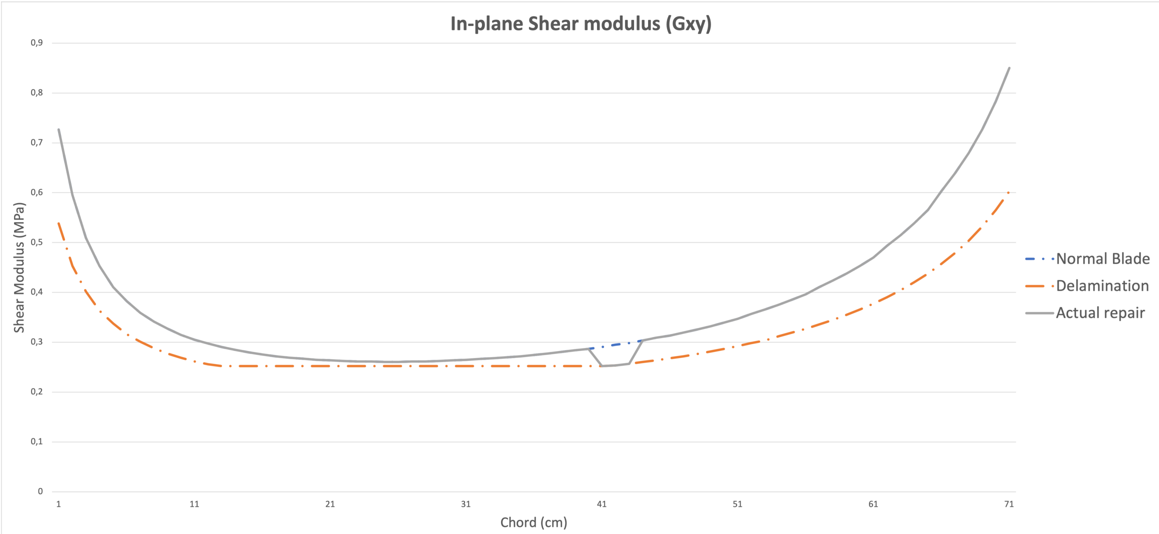

Figure 5.7: Cross sectional shear modulus with delamination

Figure 5.6 and 5.7 show that the actual delamination decreases the bending and shear modulus locally by 15%. From the simulation of the stiffness with a delamination over the whole cord length, it can be seen that a delamination towards the trailing edge at a cord length over 60 cm becomes more critical. The local stiffness reduction at the trailing edge was 25%. This outcome is in line with results found in recent literature that are described in section 2.2.1. Because of the maximum size of a delamination is 6,45 cm^2, the overall stiffness reduction over the blade cord does not exceed 1% as shown in figure 5.4.

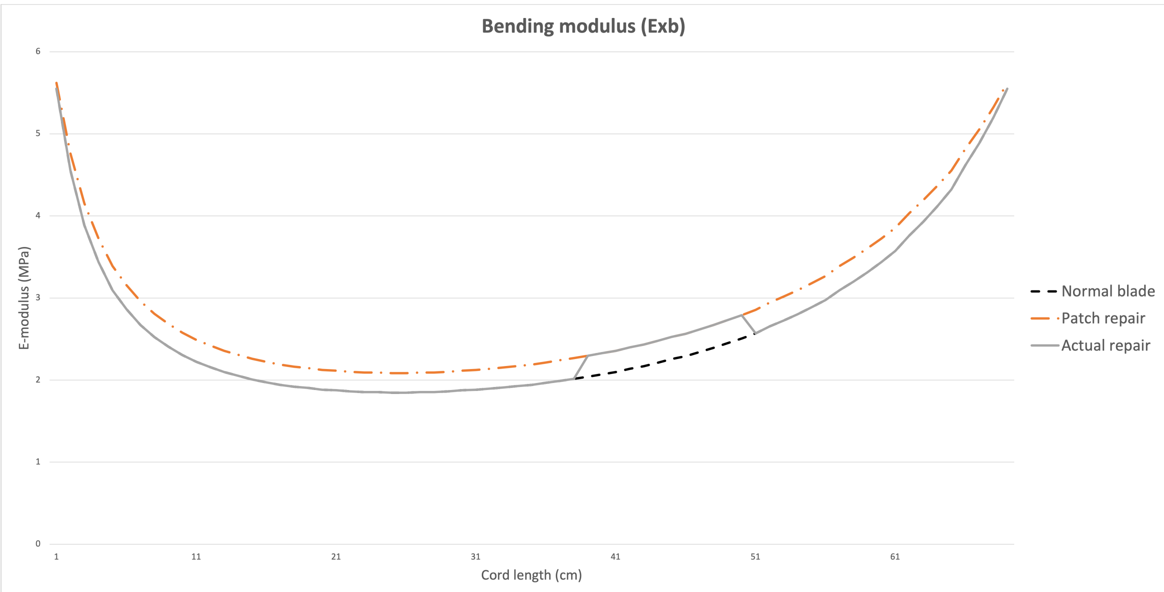

Figure 5.8: Cross sectional bending modulus with [0 90] patch repair

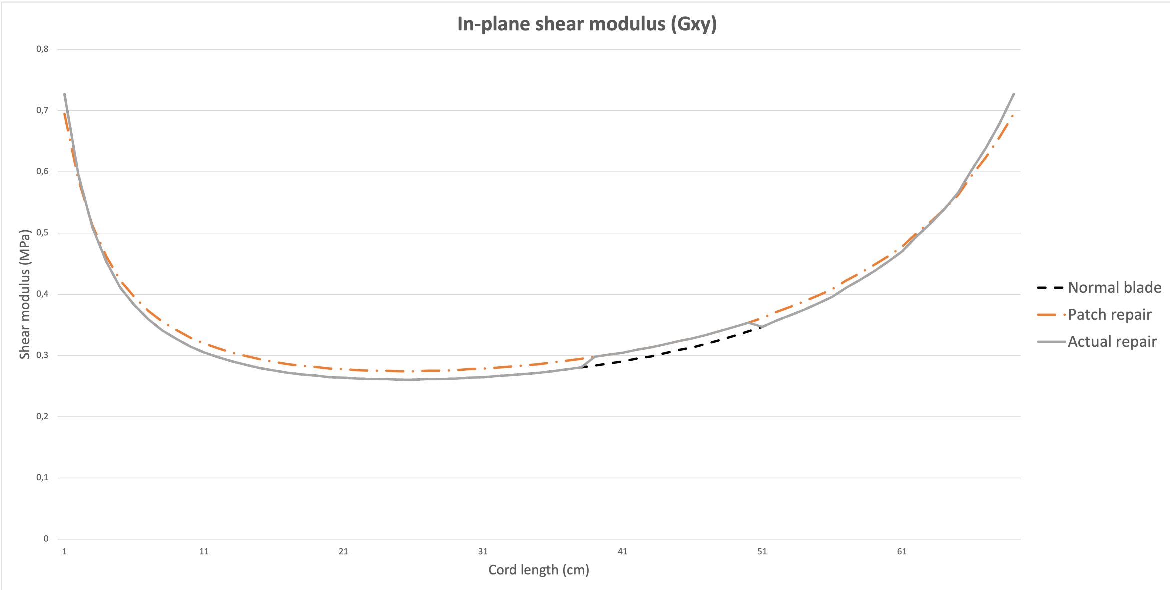

Figure 5.9: Cross sectional shear modulus with [0 90] patch repair

The [0 90] patch repair has a larger impact on the bending modulus than the shear modulus. This is expected, because ±45 plies have a better resistance to shear stress but a similar bending modulus. When the overall volume fraction of [0 90] plies is increased, this will not increase the shear modulus as much as with the application of a [45 -45] patch repair.

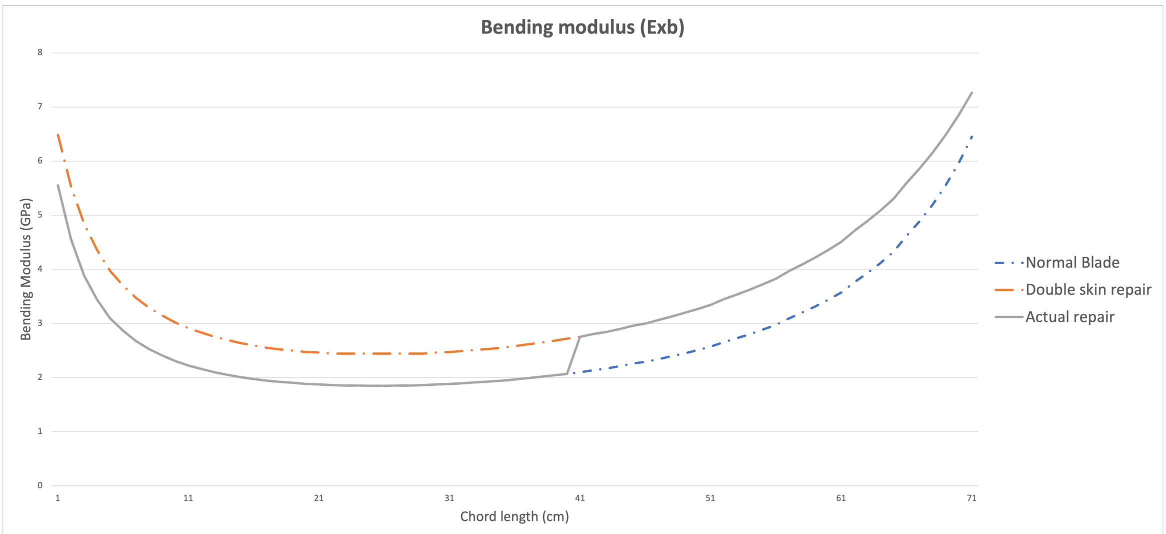

Figure 5.10: Cross sectional bending modulus with doubleskin repair

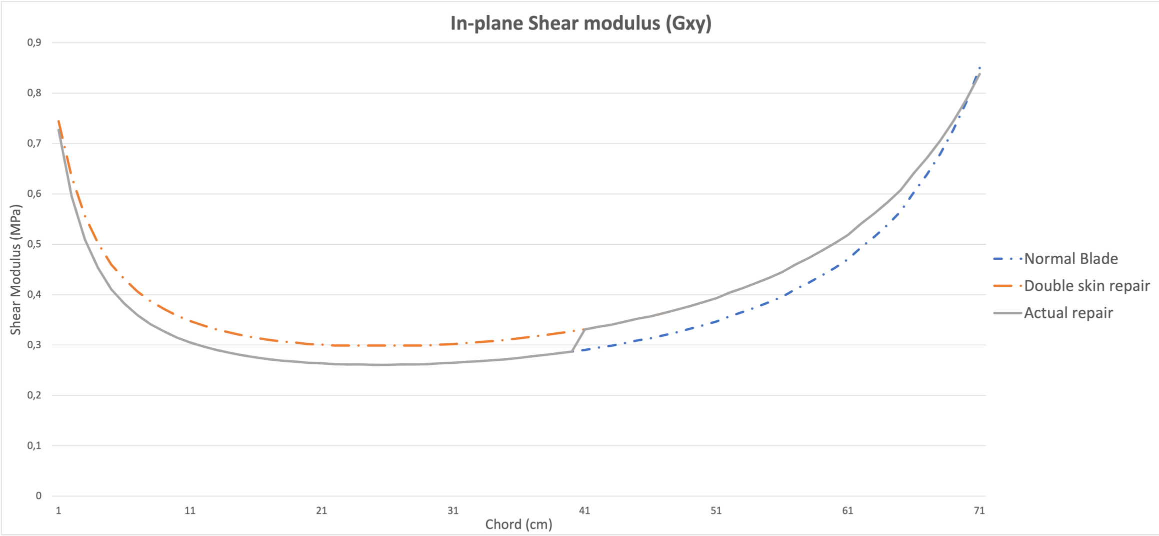

Figure 5.11: Cross sectional shear modulus with doubleskin repair

The accuracy of these calculations depends on the material properties obtained from the data sheets and the size of the non-uniformity. The influence of the uncertainty of the material data sheet is described in section 4.2.3. A deviation in the calculated material properties of ±15% was observed during the sensitivity analysis of the model. The size of the non-uniformity is obtained from the NDI images. The resolution of the camera makes it possible to determine the size of a non-uniformity with an accuracy of 0,4 mm. However, due to manual placement of the measurement point the size can be determined with an accuracy of 10 mm. A difference of 10 mm in size only affects the outcome of the calculated material property by 0,25%.

5.2.2 Model integration

The outcome of the calculations performed by the CLT model are used to improve the rotor blade FEM model that is used in the RTB simulations. The distribution of the value for the calculated material properties over the cord length are assigned to the span wise elements of the FEM model. This FEM model uploads to FLIGHTLAB and represents one rotor blade that contains non-uniformities. For the other rotor blades the standard rotor blade FEM model is used.

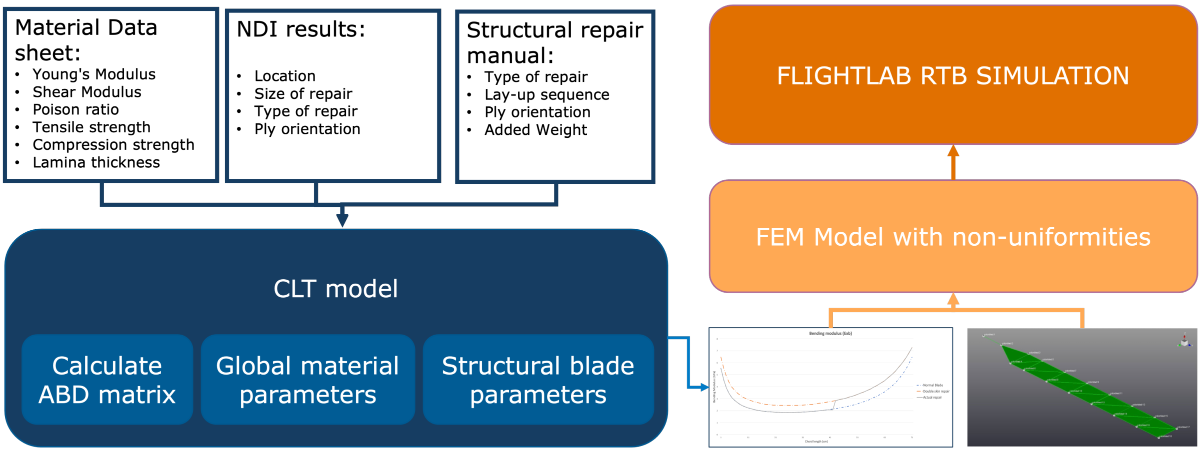

Figure 5.12: Schematic overview of model integration

The main limitation of this method is the meshing of the span wise elements. The length of the repair in the cord direction is included with an accuracy of 1 cm. The initial FEM model contained 10 elements along the span. This limited the input of the exact width of the non-uniformity. The problem was solved by increasing the mesh density to 100 elements, which give the possibility to include the width of the non-uniformity with an accuracy of 10 cm. The repair is represented as a square in the FEM model, because of this mesh grid. It is advised to further investigate the possibilities of local meshing of the rotor blade model to include the size and shape of non-uniformities more precisely.

5.2.3 RTB simulation

The RTB simulations are performed with FLIGHTLAB. FLIGHTLAB provides state of the art design and analysis software with an integrated flight simulator. This program uses selective fidelity modeling. The modeling methodologies can be adjusted based on the goal of the research to meet the requirements, while minimizing the computational cost. The model provided by the NLR consists of two three-bladed rotors in a tandem configuration. In the finite element model the rotor blades are represented as a one-dimensional beam discretized into sections along the span-wise direction. The FLIGHTLAB model simulates the rotor track and balance process as explained in section 2.1. This model is validated by Pruijsers during the ARBI Project [43]. The effect of RTB adjustments on the vibrations levels was compared to the test data gathered by Hasty et al. [9]. They collected data that consisted of in-flight vibration measurements before and after the adjustments are applied.

The RTB simulation provides the maximum vibration level in a polar plot to show the azimuth angle of the largest vibration. The delamination had a minimal effect (<1%) on the bending and shear moduli, also the size of the defect was smaller than the allowed damage size. So the delamination was not modelled in the RTB simulation. In the work of Pruijsers [43] was shown that the offset of the CG with 5% and a 10% increase of the torsional stiffness did lead to vibration levels that exceeded the maximum allowed value. To compare the result to his work the patch repair, double skin repair and an extreme case (2x double skin repair) are simulated with FLIGHTLAB. The results of these simulations are shown in the following figures:

Structural parameter	Percentual difference
Chord wise bending stiffness	+0,95%
Span wise bending stiffness	+0,95%
Torsional stiffness	+0,32 %
CG offset	+0,1% of chord

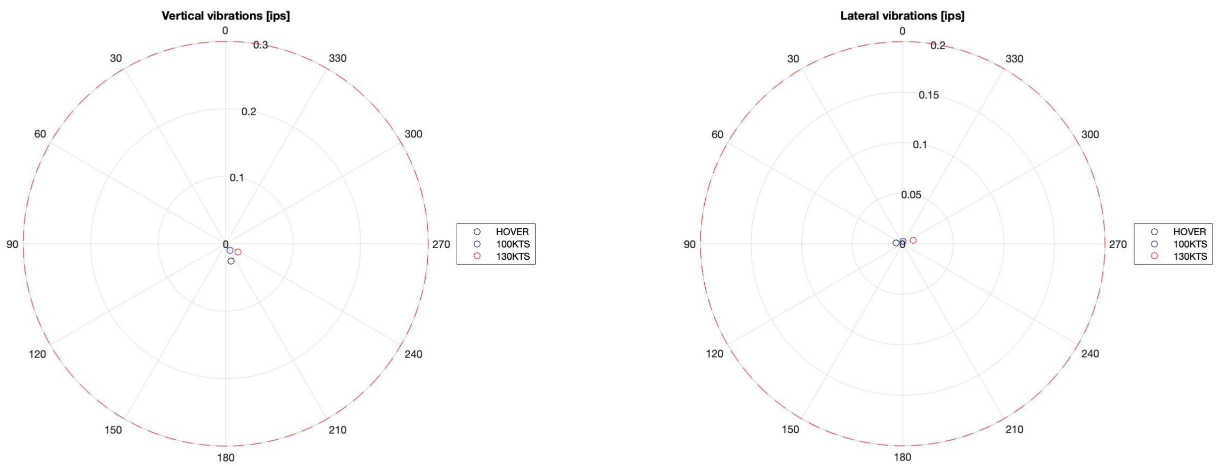

Figure 5.13: RTB vibration levels due to patch repair

Structural parameter	Percentual difference
Chord wise bending stiffness	+2,4%
Span wise bending stiffness	+2,18%
Torsional stiffness	+4,71 %
CG offset	+0,22% of chord

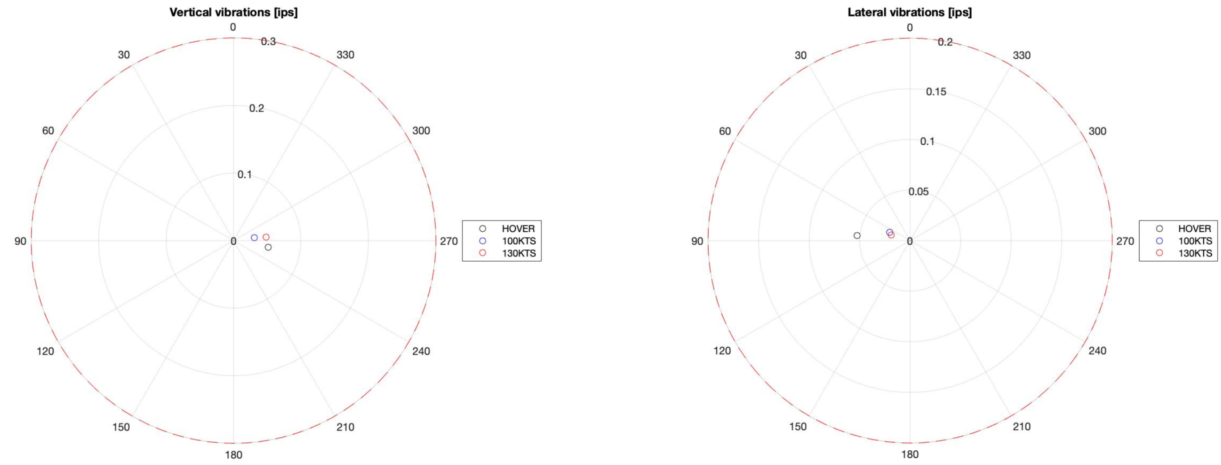

Figure 5.14: RTB vibration levels due to double skin repair

Structural parameter	Percentual difference
Chord wise bending stiffness	+5%
Span wise bending stiffness	+5%
Torsional stiffness	+10 %
CG offset	+0,5% of chord

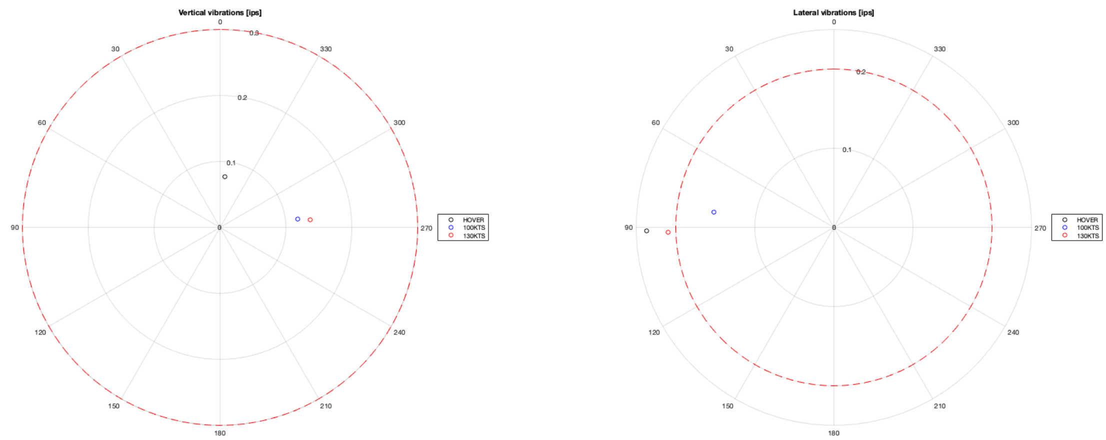

Figure 5.15: RTB vibration levels due to worst case repair at the tip section

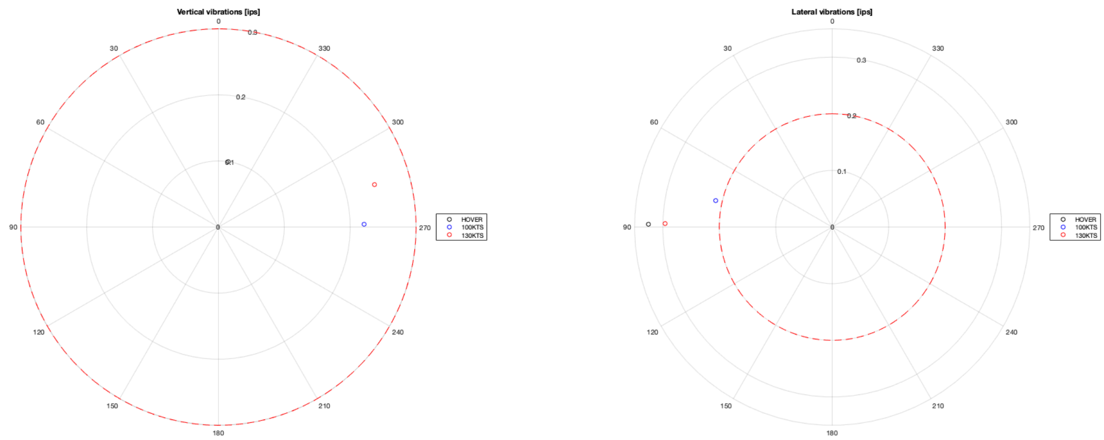

Figure 5.16: RTB vibration levels due to worst case repair at the root section

In figure 5.10 through 5.13 can be seen that the vibration levels increase with the size and impact of the applied repair. The cross sectional parameters roughly double in size for the three repair cases. For the vertical vibrations the effect looks to be linear. The effect on the lateral vibrations is linear between the patch and double skin repairs, but for the extreme repair case the lateral vibrations exceed the acceptable limits. This is in line with the findings of Pruijsers [43]. During that research was found that a 10% increase of torsional stiffness in the root section leads to a lateral vibration level in hover of 0,1 ips. The combination of an 10% increase in torsional stiffness combined with a 0.5% offset of the CG in the tip section also brings the vibration levels out of limits. The values of the extreme case are not likely to occur, but it is advised to further investigate if there is a combination of in-service defects and repairs that can lead to an increase in structural parameters similar to the extreme case. This thesis work focused on the effect of individual non-uniformities to identify their impact. It was shown that the found repairs had a larger impact on the structural properties, then the delaminations that were encountered. The impact of the delaminations was negligible due to the small size of the defect.

5.3 Conclusion

The results obtained in the rotor track and balance simulations are in line with what is expected form earlier research. In this research is shown what shift in cross section blade parameters can be expected due to in-service defects and repairs. The application of a patch repair or a double skin repair do increase the structural parameters of a rotor blade, but this does not lead to a significant increase of vibrations. In the extreme case were the structural parameters are doubled relative to the double skin repair case an exceedance of the vibration levels is observed. When the vibrations can not be brought within the acceptable limits during RTB the rotor blade which deviates the most in cross sectional parameters has to be replaced. With the method developed during this research, it can be predicted if a blade will fit in a rotor blade set and keep the vibrations within the allowed limits. It is recommended to validate the outcome of this research by simulating a complete set of rotor blades and compare the obtained vibration levels with the MSPU data of the actual RTB process.

Chapter 6

Conclusion

This chapter will summarise the conclusions from this research and provide an answer to the research questions. For convenience of the reader the research questions are repeated in this chapter followed by the conclusions that provide an answer to those questions.

- **How does the variable stiffness and change in CG of the rotor blade composite structure, caused by non-uniformities, affect the dynamical response during the rotor track and balance process?**

To answer the main question, four sub questions are formed:

1. What types of in-service damage regularly occur in helicopter rotor blades and what methods are commonly used to repair those defects?

2. Which NDI methods are most suitable for characterization of important parameters as size, thickess and depth of common in-service damage and repairs?

3. How do in-service defects and repairs alter the structural blade section parameters and chord-wise moment?

4. What is the effect of defects and repairs on the vibrations levels during RTB simulations?

6.1 Conclusions

The main goal of this research is to get a better understanding of how imperfections in the CH-47 Chinook helicopter rotor blades composite structure influence the in-flight vibration levels. This goal is achieved by performing in-service NDI inspections of CH-47 rotor blades. The defect and repairs that were found during these inspections are modeled with an assisting 2D MATLAB model based on the Classical laminate theory to improve the FEM model of the rotor blade. To test the effect of non-uniformities on the dynamical behaviour of the rotor blades, a RTB process is simulated using FLIGHTLAB.

- The main type of defect that was found during NDI were small delaminations. One butt-joint debond area was observed on the shearography images. Two types of repairs were found during the NDI inspections. A patch repair and a double skin repair.
- Delaminations were better visible on the Shearography images. Thermography showed to be superior over shearography for the determination of size and location of the non-uniformities. Butt-joint debonds were not visible on the higher frequency thermography images. A second detailed inspection at 0,1Hz was needed to identify the crushed honeycomb core area. It is advised to use shearography complimentary to thermography for damage detection, while further automation of determining the size and location of non-uniformities should be done based on thermography images.
- The patch repair and double skin repair led respectively to an increase of 0,95% and 2,4 % increase in the bending stiffness and an increase of 0,32% and 4,71% of the torsional stiffness. The center of gravity shifted by 0,1% in case of the patch repair and 0,22% by application of a double skin repair.
- During rotor track and balance simulations these non-uniformities did not lead to an exceedance of the vibration level limits. The combination of an 10% increase in torsional stiffness combined with a 0.5% offset of the CG brings the vibration levels out of limits. These levels are only achieved when a single double skin repair is applied with a core with 10x the density and carbon fiber patches instead of glass fiber. If multiple non-uniformities on a single rotorblade can lead to such increase torsional stiffness and offset of CG is not investigated.

This research showed that the presence of non-uniformties has an affect on the structural blade proporties. However, a single non-uniformities that represent in-service damage did not lead to an exceedance of the vibration levels during RTB simulations. Simulation of an extreme case showed that a blade with a combination of increase of the torsional stiffness by 10% and a 0.5% shift in location of the CG could not be balanced. The results of the NDI inspections give a detailed overview of what type of non-uniformities are found in CH-47 rotor blades. The developed 2D analytical model is able to quantify structural blade properties of a rotor blade sandwich structure with a fault margin of 15%. This model provides the ability to determine the impact of these non-uniformities on the structural parameters based on NDI results and helps to improve the FEM model that is used for RTB simulation.

6.2 Recommendations

After the completion of this research it is recommended to further investigate the following topics:

- Multiple site damage: in this research project only one non-uniformity per blade was modelled to asses the impact of different types of defects and repairs. It is recommended to investigate to what extend a combination of multiple non-uniformities affect the structural blade properties.
- Model integration: it is advised to further investigation of possibilities of local meshing of the rotor blade model to include the repair size more precisely. Also, the transition from a damaged/repaired element to the base material element could be improved by the addition of joint mechanics for the model integration.
- Validation: it is recommended to validate the outcome of this research by simulating a complete set of rotor blades that will be installed on a helicopter and compare the obtained vibration levels with the MSPU data of the actual RTB process.

Bibliography

[1] *CH-47: Vlootuitbreiding en modernisering.* URL: www.defensie.nl.

[2] M Gamauf. "Rotor track and balance: a whole lot of shaking going on". In: *Business and Commerical Aviation* (2008).

[3] A de Bruin. *Survey of techniques and presentation of a research strategy for improved procedures for the Royal Netherlands Air Force.* Tech. rep. Royal Netherlands Aerospace Center, 2010.

[4] R Ferrer et al. "New methods for rotor tracking and balance tuning and defect detection applied to Eurocopter products". In: *Annual Forum American Helicopter Society* (2001), pp. 1128–1136.

[5] T K O'Brien. "Analysis of local delaminations and their influence on composite laminate behavior". In: *ASTM international* (1985).

[6] R Ben-Ari and A Rosen. "Investigation on Helicopter Rotor Track and Balance". In: *Israel annual conference on aerospace* (1997), pp. 308–319.

[7] J Buckel. *Rotor Blade Static Balance-Art or Science.* Technical Report. Avion Inc, May 2003.

[8] M Hillmann, A Bauer, and T Rische. "Vibration analysis of rotor blades and balancing of rotors on wind turbines". In: *DEWEK Operation and Monitoring* (2004).

[9] J C Hasty, J A Keller, and S M Krick. "Improved Rotor Smoothing for the US Army CH-47D". In: *AHS International Technical Specialists Meeting on Condition-Based Maintenance* (2008).

[10] Boeing. *HC-1B Chinook Helicopter Training Package.* Boeing Rotorcraft Systems, 1958.

[11] R Ben-Ari and A Rosen. "Mathematical modelling of a helicopter rotor track and balance: Results". In: *Journal of sound and vibration* (1997), pp. 605–620.

[12] KF Fraser. *An overview of health and usage monitoring systems (HUMS) for military helicopters.* Tech. rep. Defence science and technology organization Melbourne, 1994.

[13] J Ilkko, J Hoffren, and T Siikonen. "Simulation of a helicopter rotor flow". In: *Journal of Structural Mechanics* (2011), pp. 186–205.

[14] R Ben-Ari and A Rosen. "Mathematical modelling of a helicopter rotor track and balance: Theory". In: *Journal of Sound and Vibration* (1997), pp. 589–603.

[15] M Kvalbein and T Thorvaldsen. "Non-destructive testing/inspection of composite materials-acoustic impact testing, TV holography and shearography". In: *Norwegian Defense Research Journal* (2012).

[16] A Shipsha. "Failure of sandwich structures with sub-interface damage". MA thesis. Institutionen för flygteknik, 2001.

[17] RJC Creemers. *Design and manufacture of bonded composite repairs.* Tech. rep. Netherland Aerospace Centre, 2011.

[18] S Mahdi, A J Kinloch, and M A Crisfield. "The static mechanical performance of repaired composite sandwich beams: Part I-Experimental characterisation". In: *Journal of Sandwich Structures & Materials* (2003), pp. 179–202.

[19] *Composite Materials Handbook Volume 3: Polymer matrix compsites materials usage, design and analysis.* Department of Defense USA, June 2002.

[20] M Balaskó et al. *Non-Destructive Measurement Methods (Neutron-, X-ray Radiography, Vibration Diagnostics and Ultrasound) in the Inspection of Helicopter Rotor Blades.* Tech. rep. Atomic Energy Research Institute Budapest, 2005.

[21] M Balasko et al. "Classification of defects in honeycomb composite structure of helicopter rotor blades". In: *Nuclear Instruments and Methods in Physics Research Section A: Accelerators, Spectrometers, Detectors and Associated Equipment* (2005), pp. 45–51.

[22] JH Heida and JM Müller. *In-service inspection and monitoring of composite aerospace structures.* Tech. rep. 2013, p. 26.

[23] HP Jansen and DJ Platenkamp. *Thermography on Apache rotor blade.* Tech. rep. NLR-CR-2020-067. Netherlands Aerospace Centre, July 2020.

[24] LR Kalter. "Characterisation of damage in composite materials using infrared thermography". MA thesis. University of Twente, Aug. 2019.

[25] S Kappert. "Multi-domain inspection technique for composite aerostructures". MA thesis. Hanze University of Applied Science Groningen, June 2019.

[26] M Georges et al. "Thermography and shearography inspection of composite hybrid sandwich structure made of CFRP and GFRP core and titanium skins". In: *The 18th International Conference on Experimental Mechanics* (2018), p. 484.

[27] R Montanini and F Freni. "Non-destructive evaluation of thick glass fiber-reinforced composites by means of optically excited lock-in thermography". In: *Composites Part A: Applied Science and Manufacturing* (2012), pp. 2075–2082.

[28] R Krupka, T Waltz, and A Ettemeyer. "Industrial applications of shearography for inspections of aircraft components". In: *Optical Measurement Systems for Industrial Inspection III* (2003), pp. 637–642.

[29] FLIR Systems. *FLIR SC7000 Series Technical data sheet.* Tech. rep. FLIR Systems Inc., 2014.

[30] isi-sys GmbH. *Shearography SE-sensor types.* URL: www.isi-sys.com.

[31] R Brink et al. *Feasibility studie of an Autonomous Robotic Blade Inspector.* Tech. rep. NLR-CR-2020-412. Dutch Aerospace Centre, 2021.

[32] V Dattoma et al. "Thermographic investigation of sandwich structure made of composite material". In: *NDT & E International* (2001), pp. 515–520.

[33] R Y Liang, J Hu, and F Choy. "Theoretical study of crack-induced eigenfrequency changes on beam structures". In: *Journal of Engineering Mechanics* (1992), pp. 384–396.

[34] A Morassi. "Crack-induced changes in eigenparameters of beam structures". In: *Journal of engineering mechanics* (1993), pp. 1798–1803.

[35] S P Lele and S K Maiti. "Modelling of transverse vibration of short beams for crack detection and measurement of crack extension". In: *Journal of sound and Vibration* (2002), pp. 559–583.

[36] K Aydin. "Influence of crack and slenderness ratio on the eigenfrequencies of Euler-Bernoulli and Timoshenko beams". In: *Mechanics of Advanced Materials and Structures* (2013), pp. 339–352.

[37] S Mahdi, A J Kinloch, and F L Matthews. "The static mechanical performance of repaired composite sandwich beams: Part II-finite element modelling". In: *Journal of Sandwich Structures & Materials* (2003), pp. 267–303.

[38] C Kassapoglou. *Design and analysis of composite structures: with applications to aerospace structures*. John Wiley & Sons, 2013.

[39] T Jones. *Measurements of the Bending Stiffness and Failure in 3-Point Bending of Irradiated and Non-irradiated Sandwich Beams*. Test report. University Of Liverpool, Jan. 2012.

[40] TWI. *Thermal Wave Imaging applications*. URL: www.thermalwave.com.

[41] Hexcel. *Hexcel product datasheets*. URL: www.hexcel.com.

[42] G Bender, G Yamakawa, and M Herbst. "Airworthiness and flight characteristics test of CH-47D". In: *US Army Aviation Engineering Flight Activity* (1985).

[43] Tom Pruijsers. "Modeling the Effects of Blade Dissimilarity on Rotor Vibrations for CH-47 Chinook Using a Viscous Vortex Particle Method". MA thesis. Delft University of Technology, 2021.